Icosahedral quasicrystal decoration models. I. Geometrical principles

M. Mihalkovič*
Department of Physics, Cornell University, Ithaca, New York 14853-2501
and Laboratoire de Thermodynamique et Physico-Chimie Métallurgiques, Ecole Nationale Supérieure d'Electronique et d'Electromécanique de Grenoble, Boîte Postale 75, 38402 St. Martin d'Heres Cedex, France

W.-J. Zhu and C. L. Henley
Department of Physics, Cornell University, Ithaca, New York 14853-2501

M. Oxborrow†
Department of Physics, Cornell University, Ithaca, New York 14853-2501
and Center for Chaos and Turbulence Studies, The Niels Bohr Institute, Blegdamsvej 17, DK-2100 Copenhagen Ø, Denmark
(Received 26 June 1995; revised manuscript received 26 December 1995)

It is proposed that quasicrystal structure determination should include the calculation of cohesive energies using realistic potentials. A class of atomic decoration models for *i*-AlMn is then presented, adopting the ''canonical-cell'' tiling geometry, with ''Mackay icosahedron'' clusters placed on all its nodes. The remaining atomic positions are based, as far as possible, on the known structure of α-AlMnSi. These models guarantee good local packing of the atoms, whose displacements away from ''ideal'' positions are specified by only a moderate number of parameters. Certain atomic sites are uncertain as regards their occupancy and/or chemistry; variations of the decoration rules on these sites must be compared, in order to discover the correct one. Our models are well adapted to be relaxed under an effective Hamiltonian to optimize the cohesive energy; we show how the energies found in such relaxations can be used to extract an effective tile-tile Hamiltonian, as would be needed for future studies of phason elasticity and the development of long-range order. In addition, we clarify concepts needed for decoration models in general (in particular, the ways in which elaborate, more realistic decorations may be evolved from simpler ones). We also show that these decoration models are closely related, but not identical, to quasiperiodic structures defined using six-dimensional formalism.

I. INTRODUCTION

In this paper, we motivate and then describe explicitly an ensemble of decoration models for the icosahedral quasicrystal *i*-AlMn, which are based on the canonical-cell tiling (CCT).[1] We attempt to deduce our models from what is known about *i*-AlMn, while allowing for structural variations at places in the structure where our assumptions are insufficient to force a unique structure. This was done in preparation for the systematic comparison of this entire family of models by relaxing them under realistic pair potentials; that study is reported in a companion paper,[2] henceforth referred to as paper II. In addition, the present paper includes a conceptual framework (see Secs. II and VI), which applies to decoration models quite generally.

A. Relevance to structure determination

In the past decade, many model structures based on fits to crystallographic data have been presented for icosahedral quasicrystals, such as metastable *i*-AlMnSi,[3–6] thermodynamically stable *i*-AlCuLi,[7,8] and long-range ordered, stable *i*-AlCuFe (Refs. 9–12), and *i*-AlPdMn.[13] These are formulated in terms of the six-dimensional (6D) ''hyperspace cut'' approach,[11,14] which is an economical way of describing ideally quasiperiodic structures. We believe that each these fitted structures contains a small, yet significant, residual fraction of erroneous or undetermined sites.

Let us consider *how* completely the structure must be known in order to form a reliable basis for microscopic calculations, e.g., for determining the cohesive energy (per atom) $E_{\rm coh}$. The difference $E_{\rm coh}(1)-E_{\rm coh}(2)$ between two competing structures 1 and 2, is frequently only 0.01 eV per atom. Each erroneously placed atom could easily increase the cohesive energy by ~ 1 eV, even after relaxation; thus, if just $\sim 1\%$ of the atoms in either models 1 or 2 were bad, the sign of $E_{\rm coh}(1)-E_{\rm coh}(2)$ could easily be spurious (in being determined mainly by erroneous atoms). Quite possibly, the erroneous atoms would also degrade or spoil calculations of the density of states, the conductivity, and the effective tile Hamiltonian; the latter (the subject of Sec. VI), is the input information for theories explaining the origin of long-range order in quasicrystals.

It is quite likely that the existing models *do* have erroneous atoms at the $\sim 1\%$ level, if only because of the uncertainty in the existing crystallographic data. In particular, the real-space structures contain some atomic environments of very low coordination number that are quite improbable, at least if the system is described by nearest-neighbor interatomic potentials.[15] Furthermore, we suspect that a purely crystallographic approach, by itself, will never be able to fix the positions and chemical identities of the atoms in quasicrystals to the precision required for accurate electronic-structure computations. Firstly, the usual technical pitfalls that enter the analysis of diffraction data are exacerbated in the case of quasicrystals.[16] Due to truncation effects, density maps deduced from diffraction tend to contain spurious density maxima (appearing as atoms).[17] In addition, correct atoms may incorrectly appear to lie exactly on 6D high-symmetry positions whereas their proper positions are

displaced from them.[17] Secondly, the 6D approach necessarily *assumes* that the structure has no disorder; the irreducible disorder present in all real samples is thus considered extrinsic. If, instead, local disorder were intrinsic to real quasicrystals,[18–20] then the 6D descriptions would be incomplete (in capturing only the averaged structure) and many of the principles that guide the formulation of 6D-cut models (e.g., sharp boundaries of the hyperatoms[11]) would be unreliable.

Since no single technique is powerful enough to supply us with the needed structural knowledge, we propose a ''synthetic'' approach to the problem of structure refinement, that judiciously combines complementary types of information. This involves (i) drawing analogies with known crystalline structures, (ii) fitting models to diffraction data, and (iii) insisting that models are both stable upon relaxation under realistic potentials and have lower cohesive energies than competing structures. By running cross checks of this sort, the artifacts and/or spurious features arising out of individual techniques can be detected and eliminated. Indeed, in an optimal refinement procedure, we suggest that both cohesive energies based on realistic potentials and R factors with respect to diffraction data should be calculated *in parallel*, and given comparable weights.[21] Our belief in the synthetic approach motivates and colors the present paper and paper II.

The ''synthetic approach'' could be pursued entirely within the format of the ''6D-cut'' formalism (as in the ongoing work of Cockayne and co-workers on the decagonal d-AlCo models,[22] and our own study of i-AlMn models[23]). Instead, we have chosen to adopt the ''decoration'' formalism. Decorations are based on finite-sized combinations of atoms and are formulated in 3D rather than 6D space. They thus lend themselves to easy visualization of the local patterns of atoms in the structure, which is useful if the models are to be varied and adjusted.

B. Contents of the paper

The outline of the paper is as follows. Section II introduces the general concepts upon which the decoration approach is founded—concepts which we found essential for a precise discussion, not only of each particular model, but more importantly of the *relations* between different models. In fact, we consider it an advance simply to give a precise meaning to the words ''decoration model.'' This is followed (Sec. III) by the various facts, specific to i-AlMn and canonical-cell tilings, that explain the assumptions made in the next section.

Section IV is the core of this paper. In it four families of CCT-based decoration models are presented, all of which are extensions of Ref. 24. We distinguish between those places in the structure where (we believe) the decoration is nearly inevitable, and those places where there are several plausible choices. The details of these models (in contrast to some earlier versions[25,26]) are informed by our considerable experience with relaxations under realistic pair potentials (see paper II). (Associated with Sec. IV are Appendix A, which presents an attractive and alternative way of breaking up canonical cells into smaller tiles so as to extend the α-AlMnSi decoration, and Appendix B, which describes one of our decoration models in full detail.) This is followed up in Sec. V by a discussion (summarizing Ref. 23) of the (close) relations between these CCT-based model structures and various 6D-cut model structures; here, we report the statistics of local patterns, which characterize the different structural families.

In any quasicrystal model — be it based on the matching-rule or random-tiling scenarios — the origin of long-range quasicrystal order is formulated in terms of a Hamiltonian, as a function of the tile configuration.[19,27,28] To justify such theories microscopically, and (perhaps) to test the validity of the random-tiling scenario, requires that we calculate the coefficients entering this ''tile Hamiltonian'' from the atomic structure and the structural energy function. Section VI sets up the general framework for doing this, based on relaxations of decoration models. Finally, Sec. VII ties together various ideas, presents a few suppositions and hypotheses, and describes some possible extensions to our work.

II. GENERAL CONCEPTS FOR DECORATIONS

Here, we define what we mean by a decoration model. The concepts that we introduce are quite general; they are not specific to Al-Mn chemistry, nor to canonical-cell tilings, nor to icosahedral symmetry. The section is organized around the definitions of various concepts which we found essential for understanding our work on relaxation (paper II).

A. Definitions

A ''model'' denotes a particular atomic structure. For decoration models, it means a combination of a particular tiling and a particular decoration. For six-dimensional models, it means a particular cut through a particular 6D hypercrystal. The same model can sometimes be derived via different routes. For example, variations of the ''α-AlMn'' structure appear as known crystals (see paper II), as approximants to 6D structures (see Ref. 23), and as decorations of the simple ''pure A-cell'' canonical-cell tiling. (Occasionally, ''model'' is used loosely to refer to a decoration rule.)

An ''atomic site'' is a position in space to which a ''chemistry'' is associated. This chemistry determines what (if anything) is placed at the site. In general, model structures can be formulated whose atomic sites are only partially occupied and/or contain statistical mixtures of two or more atomic species. It is difficult to relax structures of this sort in a way that leads to meaningful results. We thus elect to exclude partial occupancies and mixed species from our palette of free parameters. Each atomic site may contain only a single atom of a definite species, and this atom is either there, or it is not.

A ''tiling object'' (sometimes abbreviated to the word ''object'') is any finite, recognizable, geometrical entity within a tiling. Thus, in order of roughly increasing complexity, vertices (also referred to as ''nodes''), edges (also referred to as ''linkages,'' faces, corners (faces meeting at a vertex), tiles, ''node environments'' (the star of edges radiating out from a vertex), pairs of tiles adjoined together, or any amalgamations thereof, can all be considered as tiling objects. Each type of tiling object has a point-group symmetry, which is a subgroup of the point group that is associated with the tiling (icosahedral, decagonal, . . .).

We shall use ''differentiation'' as a general term for any modification of a simple tiling model into a more elaborate one, by simply relabeling tile objects using a deterministic rule such that the tiling configurations correspond one-to-one, and the number of tile objects increases through (at least) one type of object being subdivided into several new subtypes. This would be mathematically superfluous if we were concerned only about the set of allowed tilings; however, it is natural in a decoration model when the atomic arrangements are different on the different subtypes.

There are two common forms of differentiation:

(i) A ''context-sensitivity,'' whereby objects are differentiated according to their local environments in the tiling. Upon doing so, each tiling gives rise to a new, unique tiling, where there is a one-to-one relationship between the old and new tilings.

(ii) A ''symmetry breaking'' of the tiling's space group. The nodes of the tiling may be colored (according to their parity, for example), or arrows may be attached to edges, or handles/stubs may be attached to faces (see Ref. 1); then the point symmetries of these tiling objects will be reduced, and the number of distinguishable types of tiling object (at any given level in the hierarchy of tiling objects as listed above) will be increased. For example, a tiling with simple-icosahedral (SI) symmetry may be transformed into a tiling with face-centered-icosahedral (FCI) symmetry (see Secs. III A and VII B 1); then any given tiling may give rise to more than one different structure, depending on one arbitrary global choice as to which of the two sublattices is taken to be even and which is taken to be odd.

In a ''decoration,'' atoms are placed on tiling objects such that both

(1) every object of a given type is decorated in the same way (just like a unit cell in ordinary crystallography), and

(2) the point-group symmetry of a decorated tiling object is the same as that of the ''bare'' tiling object before decoration.

Atomic sites that decorate a given tiling object are said to be ''bound'' to that tiling object. Condition (ii) above forces atomic sites to lie in discrete ''orbits,'' generated by the point-group symmetry of the tiling objects to which they are bound. The association between these orbits and their tiling objects is called a ''binding.'' To avoid the generation of duplicate atoms, we insist that, within a given binding, each atomic site is bound to a unique orbit. The specific coordinates of atoms generated in this way, will be called the ''canonical positions'' for that model and binding.

Models are ''topologically equivalent'' if they relax to structures with identical atomic coordinates.[29] (We assume that the initial positions are close enough to the final ones that different relaxation algorithms give identical results.) A model is ''topologically correct'' if the model positions are topologically equivalent to the real ones; it is called ''crystallographically good'' if, in addition, the canonical positions are close to the ''real'' ones. For this purpose we might plausibly take the real structure to be either the true ground state of the potentials that we assume, or the experimental structure as determined by diffraction.

B. Binding and rebinding

The utility of the decoration approach in specifying atomic structures stems from the fact that it replaces the task of determining the positions and chemistries of an infinite number of different atomic sites by the task of determining the positions and chemistries of the handful of independent atomic sites (orbits) that decorate each type of tiling object. Since a practical decoration model uses only a finite number of object types, there are only a finite number of independent atomic sites, and their positions and chemistries can be specified by a finite number of parameters. This colossal simplification comes at a price: *almost* identical environments are treated as if they are *exactly* equivalent. The actual number of free parameters is determined by the binding of the decoration model.

A given canonical orbit can typically be specified by several different choices of binding. (For example, one might account for a given site by binding it to either a nearby linkage or a nearby face.) Additionally, there may be other bindings which describe different atomic coordinates yet are topologically equivalent (in that they relax to the same structure). Out of all those topologically equivalent bindings, we define the ''minimal'' binding for that structure to be the one that uses the fewest orbits.

Since the specification of a binding, in full detail, can be forbiddingly complicated, it is usually clearer to present a decoration model in a more informal fashion, which could be called a ''topological'' description. In such a description, we relax the condition that a given atom be accounted for just once; we do not specify the numerical coordinates of the atomic sites; and we specify atomic sites with reference to the most convenient tiling objects, even if these are not the objects to which the sites will ultimately be bound.

The most compelling decoration models are those that are crystallographically good yet contain few free parameters. A decoration model can be improved (albeit at the expense of increasing the total number of free parameters) by dividing each orbit into several new orbits of lower symmetry, such that the atomic environments within each new orbit are more alike. This process is called ''rebinding.'' Formally, it can be regarded as the re-expression of the tiling in terms of a larger family of tiling objects — this step is what we called a ''differentiation,'' of the context-sensitivity variety — and the decoration of these new objects in independent ways — this is the differentiation of orbits, induced by the differentiation of the tiling. Whenever we observe that two orbits in a decoration are similar to each other, we can make this relationship precise if we can consider them both as derived from a single orbit in a simplified model, via differentiation.

Rebinding may be implemented simply so that the canonical positions in an orbit may more closely approximate the real relaxed ones. Alternatively, it is possible that some of the new orbits are topologically different (here a difference in chemistry or occupancy counts as a topological difference). In either case, so as to reduce the total number of free parameters, some orbits are typically left in undifferentiated form; that is different orbits are forced to share the same canonical coordinates (as if they were bound to the original undifferentiated tile objects).

C. Canonical and ideal positions

Rather than using generic canonical coordinates, it is often convenient to adopt ''ideal coordinates,'' meaning that positions can be written[30]

$$\mathbf{r}=\sum_{j=1}^{6} n_j \mathbf{a}_j , \tag{1}$$

where the n_j are integers or half-integers and the $\mathbf{a}_j$ are six basis vectors, independent over integers and pointing towards the corners of an icosahedron; $|\mathbf{a}_j|=a_q\approx 4.6$ Å, the ''quasilattice constant.'' The vertices in an Ammann tiling and the nodes in a canonical-cell tiling always have ideal coordinates. So do the atomic sites in 6D models with flat atomic surfaces. [It is clear from Eq. (1) that ''ideal'' positions are simply the projections of high-symmetry Wyckoff sites within the appropriate 6D regular lattice.]

It is often useful to specify a canonical position as an ideal position plus a displacement.[31] Within the decoration-model approach, sites may be displaced only in directions that respect the point symmetries of the tiling objects to which they are bound; the space of canonical displacements for a given site may be either 0-, 1-, 2-, or 3-dimensional.[32] All of the models presented in this paper use ideal positions, for simplicity[33] and because they are intended merely for use as starting structures for relaxations (paper II). On the other hand, a decoration model that is destined for structural refinements must be specified in terms of generic canonical coordinates.

A laudable aim is the discovery of crystallographically good decoration models, whose atomic sites lie extremely close to the positions of the atoms in real quasicrystals. Given that a decoration model is topologically correct, the discrepancy between it and the real structure can be characterized in terms of the ''canonical rms'' σ_j for each orbit j, defined as the root-mean-squared difference between the real and canonical positions of the sites in that orbit. Optimized canonical positions can be determined by minimizing each σ_j; thus $\bar{\sigma}$, the properly weighted combination of σ_j's for all orbits, is the real-space analog of the R factor of diffraction refinements. Certainly $\bar{\sigma}$ can be decreased by rebinding atoms to newly differentiated tiling objects with lower point symmetries (since this gives the atoms a greater range of displacements to choose from), though at the expense of introducing more free parameters.

III. BACKGROUND FOR AL-MN STRUCTURES

In this section, we review well-known features of Al-Mn quasicrystals and related crystal structures, which serve as the starting point for our minimal decoration model (Sec. IV). This includes both some essential facts on the canonical-cell tiling, which will serve as the framework for the decoration model, and also some generalities about the typical local order in these alloys.

A. Canonical-cell tiling

We base our decoration models on the canonical-cell tiling (CCT).[1] Some of us have used these tilings in two previous models for FCI *i*-AlMnSi.[25,26] CCT-based models have also been produced for *i*-AlCuLi and *i*-TiMn.[34,35] The CCT packing rules permit periodic, random, or (in principle) quasiperiodic tilings;[1,36,37] no rule for a quasiperiodic CCT is yet known.

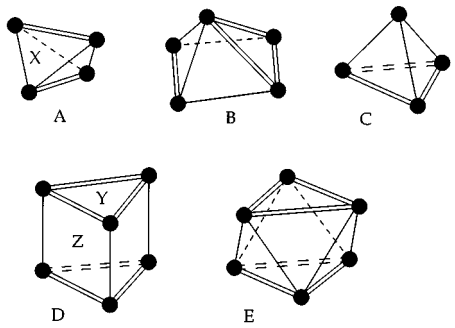

FIG. 1. The canonical cells. Edges are *b* linkages (double lines) and *c* linkages (single lines). The face names are also indicated.

Here, we recall the nomenclature and essential facts about the CCT, which will be used in Sec. IV. Canonical-cell tilings are built out of four kinds of cell, denoted *A*, *B*, *C*, *D*, such that their ''nodes'' (i.e., vertices) are joined by a network of ''linkages'' (i.e., edges). These linkages run in both the twofold and threefold directions (see Fig. 1), denoted ''*b*'' and ''*c*,'' respectively.[38,39] There are three different sorts of cell face, which have the shapes of an isosceles triangle (framed by one *b* linkage and two *c* linkages), an equilateral triangle (framed by three *b* linkages), and a rectangle (framed by two *b* linkages and two *c* linkages); these are denoted ''*X*,'' ''*Y*,'' and ''*Z*,'' respectively. Together, the nodes, linkages, faces, and cells comprise a set of ''tiling objects'' for the CCT.

Our CCT-based decoration models require one further cell, the *E* cell; this is a squashed octahedron filling the same space as two *B* cells sharing a (rectangular) *Z* face. This modification of the CCT as defined in Ref. 1 ensures that every allowed arrangement of nodes corresponds to a unique tiling.[40] The internal *Z* faces within the *E* cell are denoted ''Z_{BB}''; those *Z* faces that do not lie inside *E* cells are denoted ''Z_D,'' since they form the (rectangular) sides of *D* cells; the distinction between these two types of *Z* face is only made where relevant.

The CCT nodes are bipartite, in the sense that they can be divided into ''even'' and ''odd'' sublattices. Even (odd) nodes have integer coordinates in 6D whose sums are even (odd). Nodes connected by *b* linkages have the same parity; those connected by *c* linkages have opposite parities.

Consequently, FCI decoration models can be realized by distinguishing the even and odd nodes, and consequently various tiling objects (bonds, cells, etc.) of which these nodes form a part. Many CCT objects get differentiated into even- and odd-flavored versions, defined according to the parity of the nodes within the object. Thus a *b* bond is even (odd) when it connects two even (odd) nodes. On the other hand, the *c* bond, connecting one even and one odd node, still comes in one flavor but its ends are no longer symmetry-equivalent to each other. Other objects, important in our decorations, that acquire two flavors are the even (odd) *Y* faces [which have even (odd) nodes on all vertices], and the even (odd) *D* cells [for the orientation shown in our figures, their lowest *Y* faces are even (odd)].

B. Typical atomic motifs

Our most important (and largest) motif is the Mackay icosahedron (MI) cluster;[41] see Fig. 2. This is composed of

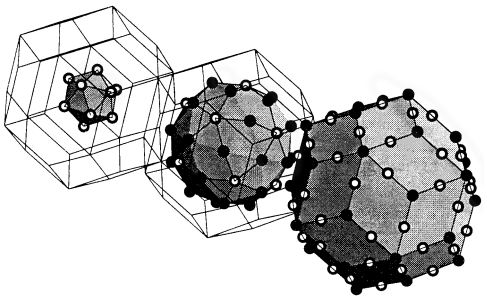

FIG. 2. Icosahedral cluster with three shells of atoms (left to right), shown within the outline of a large triacontahedron. The first two shells constitute the ''Mackay icosahedron'' (MI). Open circles are Al; filled circles are Mn (on the second shell) or candidate δ sites (on the third shell).

inner and outer shells. The inner shell contains 12 nearest-neighbor Al atoms, located at the vertices of a small icosahedron. The outer shell comprises 12 Mn atoms and 30 Al atoms: the 12 Mn atoms are located at the vertices of a larger icosahedron, about twice the radius of the small one; the 30 Al atoms are located along twofold axes, just outside of the larger icosahedron. There is good reason to believe that MI are present in *i*-AlMnSi quasicrystals from the similarity of the Patterson function to that of α-AlMnSi,[3] and perhaps also from extended x-ray-absorption fine-structure (EXAFS) results.[42] The 6D diffraction refinements are, in fact, not inconsistent with the ''6D midedge'' sites, that represent the inner icosahedron of Al atoms in the MI.[43]

Next, we mention a motif which is *not* observed in approximant crystals, but which appears commonly in many 6D cut models. The ''pseudo-MI'' is composed of inner and outer shells. Its outer shell, containing 12 Mn and 30 Al atoms, is identical to that of the MI. Its inner shell, however, contains only seven Al atoms, which are located along threefold axes radiating from the center of icosahedral symmetry. From the viewpoint of good packing, as favored by familiar nearest-neighbor potentials, such a pattern seems quite implausible. However, experience with realistically oscillating potentials (paper II) has taught us to be cautious in making such judgments.

A secondary, common motif is the ''mini-Bergman'' cluster, which consists of an $Al_{12}Mn$ icosahedron as an inner shell, plus an outer shell of 20 Al or Mn atoms on the threefold axes of this icosahedron. This cluster has been discussed as a fundamental motif for the Katz-Gratias quasiperiodic (6D cut) model.[11] It appears very frequently in a model for *i*-TiCrSi (in the *i*-TiMn family), whose characteristic local order interpolates between the Al-Mn and Frank-Kasper families of quasicrystal.[35] [The complete Bergman cluster, which is the dominant motif of bcc *T*-AlZnMg (Ref. 44) and related ''Frank-Kasper'' quasicrystalline phases,[45] differs from the mini-Bergman cluster through the presence of 12 additional atoms on the outer shell, along the icosahedron's five-fold axes.]

The energetic favorability of those motifs ought to be explained in terms of cohesive energies, hopefully expressed as effective interatomic Hamiltonians with local interactions. It might turn out that the large motifs are simply the best solutions for maximizing the frequency of some small motifs, which are discussed next.

The known, stable Al-rich AlMn alloys (including those which are not quasicrystal approximants) contain certain characteristic, repeating motifs at the scale of a single coordination shell. (Similar patterns are seen in the other Al-transition-metal alloys.) Even if the effective interatomic Hamiltonian is not available, one can gain some insight into this Hamiltonian and the probable local order in *i*-AlMn by studying these small-scale motifs;[46] the resultant conclusions are

(i) the Mn-Mn spacing is strikingly uniform[47] in alloys whose Mn concentrations (x_{Mn}) lie near the quasicrystal-forming value. The typical Mn-Mn separation in such (Al-rich) alloys is ~ 4.6 Å.[48]

(ii) The $Al_{12}Mn$ icosahedron (centered by Mn) is a ubiquitous motif. This forms the center of the ''mini-Bergman'' cluster (see below). The MI cluster (the backbone of our decoration) is a super-icosahedron formed by $Al_{12}Mn$ icosahedra.

(iii) Octahedra of Al_6 are a common pattern, prominent in the MI cluster (and its extension to a three-shell cluster,[49] see Fig. 2). Thus, in contrast to the AlCuLi family of quasicrystals, the AlMn alloys are *not* ''tetrahedrally close packed.''[50]

IV. MINIMAL DECORATION MODEL FOR Al-Mn

In this section, we present the core content of this paper: decoration models for Al-Mn based on the Mackay icosahedron (MI) motif and the geometry of the canonical-cell tiling (CCT). We limit ourselves to binary Al-Mn models (as opposed to studying ternaries, such as *i*-AlPdMn) primarily because, in paper II, we lacked the requisite effective pair potentials for relaxing ternary models.

We consider two classes of decoration rules: ''dense'' rules which attempt to optimize the atomic packing, and ''loose'' rules which, we discovered, do a better job of satisfying realistic potentials (see paper II). We also consider two kinds of ''Bravais'' symmetry: SI symmetry, as is experimentally observed in real *i*-AlMn and *i*-AlMnSi; and FCI symmetry, which is created if one takes the natural generalization of the α-AlMnSi structure,[51] and which seems to be present as *local* order[52] in *i*-AlMn. Thus, four major families of decoration may be delineated by the various combinations of dense/loose and SI/FCI.

The complete presentation of a decoration model really consists of two parts: first, a ''topological'' description, that both covers all atomic sites (possibly some of them more than once) and also has the correct bond topology, but which does not specify the precise positions of the atoms; and second, the binding, which assigns atoms to tiling objects such that none of them are duplicated, and which specifies the positions metrically. Descriptions of the former sort are the subject of this section. We present an example of a binding (viz. a minimal binding for the loose SI decoration) in Appendix B.

A. Overview

We will present the decoration rules by outlining the process by which we guessed them. For each decoration rule, we

find it convenient to distinguish ''zeroth-order,'' ''first-order,'' and ''second-order'' levels of description.[53] The zeroth-order model is formulated by decomposing the canonical-cell tiling into smaller tiles and decorating these by simple rules. The resultant structure contains a few glaring conflicts or duplications of atoms. Fixing them yields the first-order model; the process amounts to a ''rebinding,'' which implements ''context sensitivities'' (see Sec. II B).

The first-order model is usually plausible (as can be checked by stability under relaxation), but a few places are poorly packed and costly in energy. Models in which these too are fixed, as in the models actually relaxed in paper II, will be called ''second order.'' Such models include possible ''variants'' (alternate versions of the decoration, differing by the occupancy of special sites).

We adopted this stratified way of presenting models because

(i) the same general approach could be (and has been) applied to other kinds of quasicrystal;

(ii) it organizes our thinking about the different orbits — two orbits are likely to have similar local environments, if they arose by differentiation from the same orbit in the ''zeroth-order'' model;

(iii) we want to impress upon the reader that our models are not arbitrary inventions; their forms are practically inescapable, once we have assumed that the structure is a packing of Mackay icosahedron (MI) clusters arranged in a CCT geometry;

(iv) it hints at a heuristic but systematic approach to guessing more realistic models by ''differentiating'' the orbits of cruder models.

As our starting point, we demand that our decoration conform to the known features of the cubic α-AlMnSi structure (also seen in hexagonal α-AlFeSi): mechanically reproducing α-AlMnSi motifs, wherever we can, yields a complete zeroth-order model. Thus, every CCT node is occupied by a two-shell Mackay icosahedron (MI) cluster, and the configurations of atoms surrounding the twofold (b) and threefold (c) linkages are the same as in the α phase; see Fig. 2. The MI clusters include the inner icosahedron of Al(α) atoms and the outer icosahedron of Al(β) and Mn(μ) atoms. This accounts for about 70% of the atoms, in particular all those in the A cell and nearly all of them in the C cell.

From this point, there are several paths for guessing how, using the structure of α(AlMnSi) as a guide, the decoration can be extended to the interiors of the larger D and E cells; happily, they all lead to exactly the same basic decoration rules. These paths are based on two different ways of subdividing the CCT into smaller tiles:

(i) subdividing into ''vertex rhombohedra,'' such that each CCT node is a vertex, where the tips of many such rhombohedra meet.[54] (We call them ''vertex'' rhombohedra because their corners can be projected from vertices in 6D.) We shall refer to this path as the ''vertex-rhombohedral'' approach.

(ii) subdividing into ''dual'' rhombohedral objects, such that each CCT node is surrounded by an (icosahedrally symmetric) triacontahedron representing large three-shell atomic clusters. (We call these objects ''dual'' because their corners can be projected from the body-center sites in 6D.) This geometrical treatment of CCT is presented in Appendix A; we shall refer to it as the ''dual-rhombohedral'' approach.

Exceedingly simple ''zeroth-order'' models can be obtained by decorating these small tiles with orbits.[55] Decorations of this sort are, however, unacceptably crude—they typically produce conflicting pairs of atoms. Our ''minimal (first-order)'' decoration model is, in essence, a differentiation via context sensitivity (see Sec. II B) of such a zeroth-order model, the orbits of which get rebound to canonical cells (and the various tiling objects associated therewith). Our labels for orbits reflect this evolution: the Greek letter denotes the zeroth-order orbit from which the given site is descended; where needed, other subscripts distinguish particular orbits in the minimal (first-order) model. Thus orbits with the same Greek letter tend to have similar local environments and behave in similar ways upon relaxation.

In the rest of this section, we first present our minimal (first-order) model from the ''vertex-rhombohedral'' viewpoint (Sec. IV B). We then address the conflicts that arise, first those involving the ''γ'' atoms (Sec. IV C), and then those involving the ''δ'' atoms (Sec. IV D), which are responsible for the key differences between our families of model. The resolution of the handful of questionable environments within each family leads to variant decorations; these are discussed in Sec. IV E at the end.

For the specific loose models emphasized in this paper, the vertex-rhombohedral viewpoint turns out to be more succinct for describing the structure model. However, the dual-rhombohedral viewpoint is more economical for grasping the geometry of the model and (probably) for explaining its physics.

B. Vertex-rhombohedral approach

In this subsection, we will present the minimal (first-order) decoration of the vertex rhombohedra.

1. Geometry of vertex-rhombohedral tiling

It is well known that the simplest quasiperiodic tiling with icosahedral symmetry is the Ammann tiling [sometimes called 3DPT (Refs. 24, 30 and 56)]. Its tiles are the prolate rhombohedron (PR) and the oblate rhombohedron (OR); their rhombic faces are all congruent, and their edges all have length a_q and point along fivefold symmetry axes. The CCT may be decomposed in a unique fashion into PR's, OR's, and rhombic dodecahedra (RD's).[1] Collectively, and loosely, these will be called ''rhombohedra.'' This decomposition is illustrated in the case of the D cell's interior in Fig. 3; each successive layer of rhombohedra fits exactly over the surfaces of the layer below.

To each b linkage, we assign an RD, and to each c linkage, we assign a PR; we shall call them ''RD_b'' and ''PR_c,'' respectively; they both have MI's at their tips and were already encountered in Ref. 24. We assign to each triangular Y face another kind of PR (''PR_Y''), which pierces the Y face. It is useful to divide these PR_Y into two subclasses, called ''$\mathrm{PR}_Y(C)$'' and ''$\mathrm{PR}_Y(D)$,'' according to whether the cell adjoining the Y face on the side marked ''+'' (Ref. 1) is a C or a D cell, respectively (most of the PR_Y lies within the cell on that side). To each D cell, we also assign three more PR's (PR_D). And finally, to each (rectan-

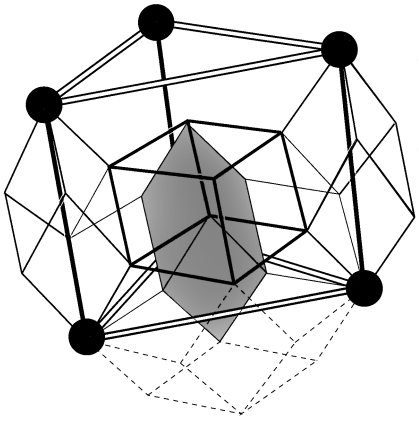

FIG. 3. Decoration of D cell by vertex rhombohedra: (1) the $PR_Y(D)$ appears shaded in the center; (2) adjoining it are two (out of the three) PR_D (thin lines), whose lower tips coincide with nodes at the bottom of the D cell; (3) centered on the rectangular Z_D face at the front is an OR_Z (bold lines); (4) two (out of three) PR_c are shown (medium lines) spanning the c linkages along the vertical sides of the front Z_D face; (5) a RD_b (dashed lines) spans the b linkage along the bottom edge of the front Z_D face.

gular) Z face, we assign an oblate rhombohedron (OR_Z), as seen in Fig. 4(b) of Ref. 1. This OR_Z also occurs at the center of the E cell. (It could also be viewed as decorating the internal Z face that arises when the E cell is divided into two

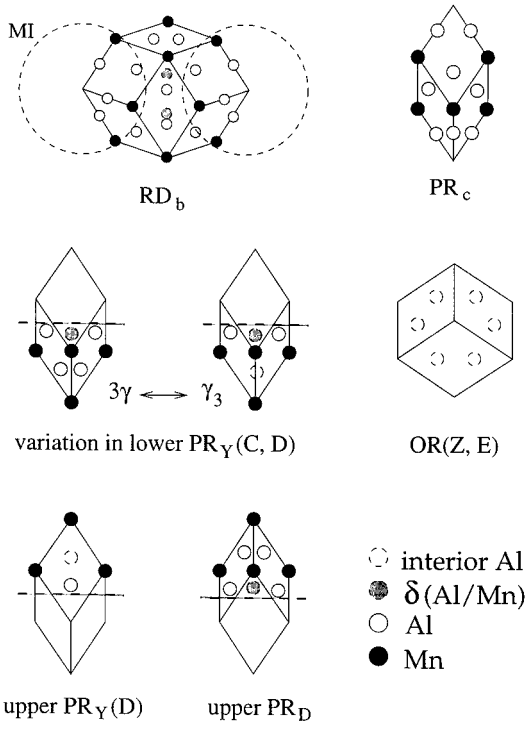

FIG. 4. Decoration of vertex rhombohedra by atoms. All δ atoms are interior; interior γ(Al) atoms inside a PR may occasionally be Mn (see text). Atoms on hidden faces are not shown. The second shell of an MI cluster is shown schematically by dashed lines at the tips of the RD_b; similarly there is an MI at each tip of PR_c. The density variation is possible for both $PR_Y(C)$ and $PR_Y(D)$. The lower half of PR_D and the upper half of $PR_Y(C)$ are identical to half of PR_c, since MI's are centered on those tips.

B cells.) In the following descriptions, we will use the words lower, upper, front, etc., with reference to the orientations of the objects shown in Figs. 3 and 4.)

2. Zeroth-order description

The zeroth-order version of the decoration is a generalization of the Elser-Henley decoration:[24]

(i) First, we decorate every CCT node with a Mackay icosahedron (MI) cluster. This fixes a good many of the atoms lying on or inside the rhombohedra that link the nodes of the CCT (viz. the RD_b and PR_c). See Fig. 4. In particular, all vertices of the MI turn out to be rhombohedron vertices ["Mn(μ)" sites in our description]. The Al atoms in the MI form the Al(α) and Al(β) sites.

(ii) Next, to decorate the b linkages, we place two Al(γ) atoms on each side and top face of every RD_b. In addition, we place two candidate δ sites in the interior of each RD_b, along its "vertical" twofold axis; we will refer to these as the "δ_b" sites. See Fig. 4. Here, we call the δ_b sites "candidate" because only some of them will be occupied; indeed, the treatment of δ sites is the key distinction between dense/loose and SI/FCI models. So as to emphasize the features that are common to all four model families, we postpone the details of δ-site occupancy to Secs. IV D and IV E.

The above rules (i) and (ii) are identical to the decoration of a pure A-cell tiling, as described in Ref. 24. This A-cell tiling is special, in that it can be decomposed into PR_c and RD_b, and no others. More general canonical-cell tilings necessarily contain other rhombohedra, whose decorations we have yet to specify.

Several of these other rhombohedra have tips that lie at CCT nodes. For example, the top tip of each PR_Y lies at the apex of a C cell, and the lower tips of each PR_D triplet lie at the three lower corners of a D cell. The decorations of such tips are determined by the decoration of each CCT node with an MI. Furthermore, the decorations on the top and side faces of the RD fix the decoration on the faces of the other rhombohedra adjoining it.

Thus, the decoration of the remaining rhombohedral faces can be summarized by the following two rules, which are generalizations of the way in which the RD_b faces are decorated:

(iii) We place a Mn(μ) atom on *every* rhombohedron vertex that was not already covered by rule (i).

(iv) Next, we place two "Al(γ)" atoms on the long diagonal of every rhombic face, except when one endpoint is a CCT node. [In that case, the face decoration is already specified by rule (i).]

On the three upper faces of $PR_Y(D)$, the Al(γ) atoms form two sets of trios; we name the upper trio, which lies nearer to the upper PR tip, "γ_{D2}," and the lower trio, which lies nearer to the PR center, "γ_{D1}."

Finally, we decorate the interior of the PR.

(v) To each $PR_Y(C)$, we place a δ_Y site on its long (threefold) axis in the end lying closest to the Y face, such that the site divides the long axis in about the ratio $\tau^{-1}:\tau^{-2}$; similarly, we place a δ_D site in the upper end of each PR_D.

A simple rule to codify the asymmetry in the placement of these (candidate) δ sites is that they may reside only in those ends of PR which do not have a Mackay icosahedron (MI) cluster at the tip. Thus, PR_c, with an MI at both its tips, can contain no δ site, while the $PR_Y(C)$ and PR_D can each host

one δ site (in the ends whose tips do not coincide with the apex of the surrounding C cell, and a node at the bottom of the surrounding D cell, respectively). The placement of an (occupied) δ site in $\mathrm{PR}_Y(D)$ is precluded by the presence of the γ_{3D} site (see below), which lies nearby and also on the threefold axis. We remark here, that the placements of candidate δ sites would seem to be more natural from the ''dual-rhombohedral'' viewpoint (see Appendix A). This completes the zeroth-level decoration rule.

C. Resolving γ atom conflicts: First-order description

The zeroth-order decoration produces two kinds of conflict between the γ sites that are generated by rule (iv); both are resolved in the first-order decoration. At the same time, we note some remaining options for these ''problem places,'' which provide some of the variations in Sec. IV E.

The first kind of conflict concerns the OR_Z, which, in the zeroth-order decoration, gets six ''Al(γ_Z)'' sites on its top three faces and six on its bottom three faces. These sites form extremely close pairs, so close that they must be merged, producing a hexagon of Al(γ_Z) sites, which lie in the plane bisecting the short axis of the OR_Z. These sites are called ''γ_Z,'' since there is one such hexagonal ring of sites for every Z face.

It is not obvious, but it emerged from relaxation studies (paper II) that even the γ_Z ring is somewhat overpacked. This is resolved, not by merging these sites, but by leaving some of them unoccupied; this leads to the ''4/6'' and ''5/6'' variants (the numerator indicates the number of sites that are occupied). The symmetry imposed by our use of deterministic decorations prevents us from implementing such variants in many places; for example, the $\bar{3}$ symmetry of the E cell demands that we use the ''6/6'' option (all six sites occupied) for the γ_Z sites associated with the $\mathrm{OR}_Z(E)$ inside that cell.

The second kind of conflict concerns the PR tips that do not coincide with CCT nodes. These tips receive a triangle of Al(γ) atoms lying too close together (their separation is roughly $\sim\tau^{-1}$ of the usual interatomic distances). Such triangles have two possible fates:

(a) in the ''3γ'' option, all three sites remain — in the real structure they must of course relax outwards somewhat from the faces of the PR;

(b) in the ''γ_3'' option, the triangle of γ sites is merged into a single γ_3 site.

At the upper tip of PR_D, we always (in every decoration rule) take the 3γ option. At the upper tip of $\mathrm{PR}_Y(D)$, on the other hand, we take the γ_3 option, collapsing $3\gamma_{D2}\rightarrow\gamma_{3D}$. The only PR tips not yet considered are the lower ends of PR_Y. Here, we take the 3γ option in the ''first-order'' rule, but in some variant (''second-order'') models these atoms can form a γ_{3Y} site instead; the choice is influenced by the neighboring atoms, in particular by the occupancy of the surrounding δ atoms. (Thus, in the complicated variants of the ''dense'' FCI models, different resolutions of the γ triangle give rise to ''even'' and ''odd'' flavored decorations of the PR_Y's.)

This completes our first-order description. We chose to force the first-order model to be virtually the same for all combinations of the dense/loose and SI/FCI attributes, in order to highlight the similarities between these models. We will now turn to the differences.

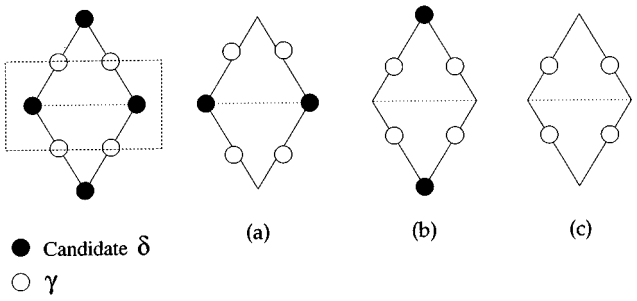

FIG. 5. Conflicts between δ atoms as mediated by γ atoms. The rhombus (divided into two isosceles triangles), with edges of length $a_q\approx 4.6$ Å, is part of the δ network. The dotted rectangle on the left most rhombus is the outline of a rhombic dodecahedron, viewed down its long axis. In (a) and (b) the δ-δ spacing is $1.05a_q$ and $1.70a_q$, respectively, characteristic of dense FCI and loose FCI decorations; in (c) all δ sites are vacant, as can occur in loose SI decorations.

D. Resolving δ-site conflicts

The candidate δ sites form a network such that the closest sites are separated by a_q (rhombus edge length), which we will call a δ link. (It is seen in Appendix A that the δ links are precisely the edges of the dual rhombohedral objects.) The issue at hand is the occupancy of the network of δ sites. As we will explain shortly, the δ atoms can be thought of as a lattice gas which satisfies an effective hard-core constraint, where the minimum separation between δ atoms is r_δ. The dense and loose models are those with $r_\delta=1.05a_q$ and $r_\delta=1.70a_q$, respectively; the dense models attempt to maximize the occupancy of δ sites under this constraint, whereas the loose models occupy an arbitrarily small fraction of them — the rules called ''LS3'' in paper II have no occupied δ sites at all. Given a particular density of δ sites, the FCI and SI models represent two different solutions to the problem of satisfying the hard-core constraint.

These δ-δ exclusions are not direct conflicts, since r_δ is much larger than an interatomic distance; rather, conflicts are mediated by the intervening γ atoms. To understand the interplay between these δ and γ sites, let us consider the rhombus of four nearby δ sites, as shown in Fig. 5; this configuration is a typical pattern in the δ network. [In the dual-rhombohedral description (Appendix A), this rhombus is the face of a dual tile; such a face lies in the plane bisecting a b linkage; now, in the vertex-rhombohedral description, this plane cuts the RD_b spanning the b linkage; the intersection of the plane with the surface of the RD_b is indicated by the dotted rectangle in Fig. 5.] The solid edges are δ links of length a_q, and the dotted edge is of length $1.05a_q$. There are γ atoms on each δ-link edge and candidate δ atoms on every corner.

First, two δ atoms connected by a δ link should not both be occupied, since that would leave too little space for the γ atom which sits near the midpoint of every δ link.[57] In Fig. 5(a), this is achieved by leaving the apex δ sites vacant and occupying the other two δ sites; such a configuration, with

closest approach $r_\delta = 1.05 a_q$, is typical of a dense model. (For the dense SI case, this constraint is not perfectly satisfied as there are rare pairs of sites with separation of only $1.0 a_q$.)

Second, although the configuration in Fig. 5(a) avoids the direct γ-δ atom conflicts, the γ atoms on edges will be displaced (upon relaxation) along the edges towards the vacant δ sites, and thus closer towards each other; the squeezed γ atoms cannot deviate very far from the rhombus edges, since there are typically other nearby atoms in such directions. Thus, Fig. 5(b) is a better configuration, with the apex δ's occupied and the other two δ sites vacant. This is typical of a loose model, where $r_\delta = 1.70 a_q$, the length of the long rhombus diagonal in Fig 5.

To implement δ-δ exclusion everywhere, the dense FCI decorations allow only even δ sites to be occupied[58] (thus, only about half of the available δ sites are filled). In other words, the lattice gas of δ's satisfies the indirect exclusion through a (global) *symmetry breaking*. In the dense SI decorations, on the other hand, δ sites are occupied (or not) according to their locations with respect to the CCT. But the whole discussion suggests that it is actually preferable to fill much less than 50% of the δ sites on average, as in the loose models, in which frequently all three δ sites in a triangle are left vacant [as shown in Fig. 5(c)]. In that case, these constraints have many solutions — the ''lattice gas'' really does have the freedom of a gas.

E. Second-order description: Families of decoration

The first-order description has fixed most of the problematic atomic orbits. The further treatment of δ sites leads to the four basic families of decorations, as has been outlined just above. Variations within each family arise from the various options that are available for resolving the problematic γ sites, as well as from the details concerning how δ sites are treated within the basic pattern of each family.

Let us review the first-order sites which are common to all our decoration families:

(a) One MI at each CCT node, consisting of Mn(0), Al(α), Al(β), and Mn(μ);

(b) Mn(ν) at each remaining rhombohedron vertex;

(c) Al(γ) pairs on each remaining rhombus face, with those on OR_Z merging into a ring of six γ_Z sites, and those around the upper tip of $PR_Y(D)$ merging into a (single) γ_{3D} site.

(d) Candidate δ_b, δ_Y, and δ_D sites in each RD_b, in the lower end of each $PR_Y(D)$, and in the upper end of each PR_D, respectively. For future convenience, the δ_b sites are divided into ''$\delta_b(A)$,'' which fall into A cells, and ''$\delta_b(BD)$,'' which fall into all other cell types (the cases are B/E or D).

The uncertain places, available for variation in the second-order description, are

(i) every candidate δ site (Al, Mn, or vacant);

(ii) 3γ sites in the lower end of PR_Y (the γ_{3Y} option);

(iii) the hexagonal ring of six γ_Z sites in each Z_D face (the ''4/6'' or ''6/6'' options).

Most of the above options are, *a priori*, equally plausible. The optimal choice might depend on the potential used, or on how other nearby uncertain sites are resolved. The variants we consider here were partly preselected on the basis of the relaxations presented in paper II:[59] we have eliminated from discussion those variants that turned out, in all situations, to be unstable under relaxation.

TABLE I. Four families of decoration rules.

Orbit	LS [a]	LF	DS	DF
$\delta_b(A)$	0	0.5	0.8–1[b]	0.5
$\delta_b(BD)$	0	0	0	0.5[b]
δ_Y	0–1[b]	0.5	0–1[b]	0.5
δ_D	0	0	1[b]	0.5[b]
γ_b [c]	1	1	1	0.90–1
$\gamma_Z(Z_D)$	0.67–1	1	1	1
$\gamma_Z(Z_E)$	1	1	1	1
γ_{D1}	1	1	1	1
γ_{3D}	1[b]	1	1	1

[a] L/S=loose/dense, S/F= SI/FCI.

[b] Sites for possible Al/Mn variation (all others in table contain pure Al).

[c] Includes γ_{3Y} sites.

We will organize our account of the variants systematically by their effect on the total number density $\rho_{\rm at}$ and on the stoichiometry (i.e., the fraction of Mn, $x_{\rm Mn}$). First, all three kinds of uncertain place allow density variations. As for chemical variations, the main option is Al $\rightarrow$ Mn on δ sites. These sites have icosahedral Al_{12} coordination shells, and $Al_{12}Mn$ icosahedra are indeed favorable motifs (see Sec. III B). On the other hand, the Mn(δ) sites do not fit well with the structural tendency to uniform spacing of Mn, as realized by Mn(μ/ν) at the corners of vertex rhombohedra; instead, the Mn(δ) option often creates Mn-Mn neighbor pairs, which is somewhat contrary to structural tendencies in Al-transition-metal alloys. There are also possible Al/Mn variations on the γ_{3D} sites among the loose SI decorations.

We are now ready to present the basic choices made by the variants in each of the big families of dense FCI, dense SI, loose SI, and loose FCI. (See also paper II.) Table I summarizes all four families of decoration rule, by showing the occupations of δ and γ sites relative to the first-order sites common to all models. Sites where a range of occupancies is shown are the candidates for density variations; when this is a fraction, it is accomplished by differentiating subclasses (implemented through a rebinding.) Note that no variants of the LF family have been defined.

1. Dense FCI models

The FCI rule is a natural generalization of the δ site behavior in α-AlMnSi:[49] the even ''candidate'' δ sites are occupied and the odd ones are vacant. Consequently, except for a few vacant δ sites due to the presence of a PR_Y, all even nodes receive third shells like those shown in Fig. 2 (the first two shells being the MI), while the odd nodes are decorated only by two-shell MI clusters. The presence of the three-shell clusters makes the dual-rhombohedral approach in Appendix A appealing for describing FCI cases, since the atoms on the third shell can be economically described by a rhombic triacontahedron.

The dense FCI case is the only decoration rule where we possibly merge $3\gamma \rightarrow \gamma_{3Y}$; this is considered for only the even Y face, since the γ sites are squeezed by the six surrounding δ_b sites (which are all occupied in the even case). This γ_{3Y} is the only ''problem site'' at which density variations are allowed for variants within the dense FCI family.

Some δ sites can be decorated either with Al or Mn. First, the δ sites originally bound to the b linkage are rebound to different cells. We then choose $\delta_b(B)$, $\delta_b(D)$, and δ_D as three sites whose chemistries (either Al or Mn) may be varied within this family of decorations. We pursued only two of the possible combinations in paper II: either all Al or all Mn on all three sites.

2. Dense SI models

Dense SI decorations can be thought of as adaptations of FCI decorations: For each type of object, we adopt either the even-flavored or the odd-flavored version of the FCI decoration rule (usually the one that is lowest in energy) and then use it for *all* objects of that type, irrespective of whether they are even or odd.

Thus, from the dense FCI decorations, we find that both the odd Y face and the odd D cell are more favorable than their even counterparts. Consequently, we fill the δ_Y site in $\mathrm{PR}_Y(C)$, take the 3γ option for both subclasses of PR_Y, and fill the δ_D site in the PR_D.

We have two candidate δ_b sites from each b linkage, but if these were all filled, they would violate the effective δ-δ exclusion at distance a_q. To prevent most of these conflicts, we simply fill only those δ_b sites which fall into A cells.

For correct accounting of these δ_b sites, we are forced, in the dense SI model, to implement added context sensitivity. The subset of δ_b sites fall into A cells will collectively be called $\delta_b(A)$. [Note that the relevant b linkage is always situated on the relevant A cell as the edge shared by the two faces marked ''$-$'' in Fig. 1(b) of Ref. 1.] Then the δ_b sites are divided into three subclasses according to what kind of cells adjoin the A cell along the two faces sharing the relevant b linkage:

(i) $\delta_b(A_4)$, when the relevant b linkage is entirely surrounded by A cells;

(ii) $\delta_b(A_2)$, when one of the adjoining cells is an A cell;

(iii) $\delta_b(A_{CC})$, when both of the adjoining cells are C cells.

Noting that δ_Y may be in δ-δ conflict with some of the $\delta_b(A)$ sites, some variants fill all the $\delta_b(A)$ but none of the δ_Y, while our densest variant among the dense SI models fills all the δ_Y and as many nonconflicting $\delta_b(A)$ as possible.

Among the many combinations of the filling of δ_Y and the three subclasses of the $\delta_b(A)$ sites, as well as the chemical choice of Al vs Mn at each site, we have extracted several representative variants which are described in detail in paper II.

3. Loose SI models

The loose SI family is similar to the dense SI family in the arrangement of its γ sites. However, in the loose decorations, most δ sites are vacant. We keep the $3\gamma_b$ option in the PR_Y, and occupy the nearby δ_Y site; this follows the example of the α-AlFeSi crystal structure.[60] We leave *all* δ_b and δ_D sites vacant; only the δ_Y sites remain as candidates. Since we no longer have the δ_b sites, we need not be concerned with the three subclasses of $\delta_b(A)$ sites, that appear above in the definition of dense SI models.

The options for variation stem from (i) the occupation/chemistry of the δ_Y site; (ii) the occupation of each ring of six Al(γ_Z) sites (only the ''4/6'' and ''6/6'' options are allowed by symmetry); and (iii) the chemistry of the γ_{3D} site in the top part of $\mathrm{PR}_Y(D)$.

An independent modification, increasing both the density and the Mn content, is to place an Mn atom at the center of every MI [this orbit is named ''Mn(0)'']. This option was favored by our potentials (paper II). The loose SI models are energetically favored in relaxations with realistic potentials, as is extensively described in paper II.

4. Loose FCI models

The basic principle of these decorations is to select a subset of the δ network satisfying the constraint $R \geqslant 1.7a_q$, and then occupy the even atoms of this subnetwork. Though we did not investigate such models in paper II, we describe one of them here for the sake of completeness.

All even δ_Y atoms are occupied. About half of the even δ_b atoms, viz. those that fall into (i) A cells or (ii) the top halves of the 3 RD_b's that frame the Y face of the D cell, are also occupied. We remark here that the δ network of the loose FCI decoration for the 3/2 CCT approximant is identical with the δ network of the 3/2 approximant to the Katz-Gratias 6D model.[11] Apart from the δ network, the loose FCI and SI decorations are topologically equivalent; thus, in the loose FCI case, the interiors of the D and E cells are still decorated the same way irrespective of whether these cells have even or odd flavor.

V. COMPARISON OF CANONICAL-CELL AND SIX-DIMENSIONAL MODELS

Having completed the specification of our decoration models, it is appropriate in this section to understand some of their properties. In particular, it is natural to ask how they fit into the more standard 6D-cut formalism[11,14] (and how they relate to well-known models defined in terms of that formalism). First, we introduce the particular 6D models that we have adopted as standards. (In a separate work,[23] we have relaxed these standard models for i-AlMn under the same potentials used in paper II.) Next, we contrast certain physical-space features of these 6D models with our CCT-based decoration models. Finally, we relate — as far as is possible — the various atomic sites in our decoration models (labeled by Greek letters) with the hyperatoms of the 6D models.

A. Description of 6D models

We adopted three ''standard'' models: (i) the Duneau-Oguey (DO) model,[4] which was originally constructed to contain MI (though the density of MI in the DO model is lower than in CCT-based models); (ii) the Katz-Gratias (KG) model structure for i-AlCuFe,[9–11] whose chemistry we adjusted[61] in order to model binary i-AlMn; the FCI modulation that this model exhibits is due primarily to 6D body-

TABLE II. Statistics of various decorations.

Models[a]	ρ_{at} (atoms/a_q^3)	N_{envt}	Z (Range)	Z (Typical)[b]	Z (Mean $\bar{Z}$)
DS	6.53–6.69	28–31	10–16	(10–14)	11.98–12.42
DF	6.67–6.77	28–38	10–16	(11–15)	12.36–12.48
LS	6.34–6.54	18–24	9–14	(10–13)	11.84–12.15
KGme	6.54	28	8–14	(11–14)	12.47
DO	6.41	34	8–14	(11–13)	12.19
KG	6.12	18	7–13	(10–13)	11.82

[a]Each model here is represented by tiling $T8$ (a 5/3 $P213$ approximant); see paper II.

[b]"Typical" means excluding the 5% with largest and the 5% with smallest coordination numbers.

center hyperatoms (corresponding to δ sites in our CCT-based decorations) that are present only on the even sublattice; and (iii) a modified version of the Katz-Gratias model in which pseudo-MI clusters are replaced by MI clusters; we call this the KGme model because it contains midedge sites.

The DO model has SI symmetry; the KG and KGme models both have FCI symmetry. For each model, as in our decoration models, there are certain sites (especially among the 6D body-center atoms, i.e., the δ sites) which lend themselves to variations of occupancy or chemistry. All three 6D models include a number of environments of low coordination number (see Table II); at least some of these environments would be expected to give rise to high local energies.

B. Comparison of physical-space features

Here, we compare our various CCT-based decoration models, both to each other, and to the three standard 6D-cut models, in terms of the characteristic local patterns in physical-space and their statistical frequencies.

Table III lists the various interatomic spacings allowed for a first-neighbor bond in the ideal versions of our models. The pair of Greek letters associated with each bond length indicates the types of atomic site that are located at the two ends of the bond in question. This table should be helpful in identifying 6D models that are similar to our decoration models and/or for making comparisons with experiments [e.g., EXAFS (Ref. 42)] that produce pair-distribution functions.

Table II contrasts various properties of three families of decoration model (the first three rows) with those of the three 6D models introduced above (the last three rows). Here, DS, DF, and LS, stand for dense SI, dense FCI, and loose SI, respectively. The variant with an Mn(0) atom at the center of every MI was adopted for all loose models quoted in these tables, including the DO model (this is the only respect in which our DO model differs from the model of Ref. 4). Here N_{envt} denotes the number of different types of local environment,[62] Z denotes the coordination number, and $\bar{Z}$ the mean of Z over all atomic sites.

TABLE III. Allowed bond lengths between ideal sites.

Orbits of endpoints	Length (a_q)
(μ,α), (δ,γ^*)	0.500
(α,α), (γ^*,γ^*)[a]	0.526
(ν,ν), (γ,γ), ...	0.563
(ν,γ^*)	0.596
(μ,δ)	0.618
(μ,β), (ν,γ), ...	0.650
(α,β)	0.679

[a]γ^* means a 6D body-center midedge site.

Extremely loose sites with coordinations under 10 occur only in the 6D models, and in our loose decoration models; presumably, some of the "neighbors" of these sites are pseudovacancies. Coordinations over 14 arise only in our dense decoration models; these tend to exhibit a large number of different types of local environment.

Much of the model geometry can be described simply in terms of two basic motifs: the Mackay icosahedron (MI) and the mini-Bergman cluster. To quantify this statement, and to check whether these two structural motifs have equal significance, we calculated the fractions of atoms that compose MI and mini-Bergman clusters for each of the three 6D models. In the KGme model with filled MI centers, a fraction 0.69 of the atoms belong to mini-Bergman clusters and a fraction 0.66 of them belong to MI clusters, while over 0.90 of them belong to at least one cluster of either type. (In the unmodified KG model, a fraction 0.79 of the atoms belong to mini-Bergman clusters.[11])

C. Comparison of 6D features

Here, we discuss the ways in which our decoration models are related to the 6D-cut models, from a 6D perspective. As a starting point for the discussion, consider an atomic model that is generated by applying a decoration rule to a quasiperiodic tiling, where every atomic site is specified using ideal coordinates, in the sense of in Eq. (1). A model of this sort can be represented as a cut through a periodic 6D structure containing "hyperatoms." These hyperatoms can be identified with pieces of 3D hyperplanes, which lie exactly parallel to the "perp" direction, and which are attached to high-symmetry Wyckoff positions within the 6D cell. Thus, the use of ideal positions within decoration rules — as is the case for our CCT-based decoration models — reveals the correspondences between the hyperatoms of 6D models and the orbits of decoration models. We should not, however, expect to find an exact mapping from our decoration models to familiar 6D-cut models: a fairly simple decoration of a fairly simple quasiperiodic tiling can easily correspond to a quite complicated 6D structure (in that the boundaries of the hyperatoms are fragmented into many small facets).

A technical advantage of decoration models over 6D-cut models is that they continue to specify well-defined positions, even on tilings that are not quasiperiodic. In particular, they can be used directly to construct periodic approximants, without the technical burden of properly shearing the cut plane and redefining the shape of atomic surfaces — as is the case with 6D models. Furthermore, we can apply the decoration to random tilings; in principle at least, this affords a more precise way of fitting diffraction data than the simple insertion of a "phason Debye-Waller" factor.

Broadly speaking, the DO and KGme models are similar to our loose SI and loose FCI decoration models, respec-

TABLE IV. Orbits in SI minimal binding.

Object	Orbit	Atoms	6D position[a]
Node	(0)	1 Mn	v
	α	12 Al	ME
	μ	12 Mn	v
	β	30 Al	v
b linkage	γ[b]	4 Al	v
Y face	ν	1 Mn	v
	δ_Y	1 Al/Mn	BC
E cell	γ_Z	6 Al	BCME
Z_D face	γ_Z	6 or 4 Al	BCME
D cell	ν	3 Mn	v
	γ_D	3 Al	v
	γ_{3D}	1 Al/Mn	v

[a]v = vertex, BC = 6D body-center, ME = 6D midedge, BCME = 6D midedge between body centers.
[b]On the hidden PR faces in RD.

tively. To make these relations precise, it is desirable to make correspondences between particular orbits in our CCT-based decoration models and particular hyperatoms in the 6D-cut models. Such identifications between classes of atom may be approached in two ways: the first is to imagine a quasiperiodic CCT-based model expressed as a 6D-cut; the second is to take an approximant to a quasiperiodic 6D-cut model and express it as the decoration of a CCT.

1. CCT orbits in 6D

Let us consider the 6D-cut representation of a decoration rule applied to a (still hypothetical) quasiperiodic CCT. First, we identify the 6D Wyckoff position to which a particular orbit is attributed by inspecting the ''ideal coordinates'' of the orbit's atomic sites (the results are included in Table IV).

The 6D vertex hyperatoms contain the MI-center [''Mn(0)''] sites, and then Mn(μ), Mn(ν), Al(β), and Al(γ) type atoms, roughly from inside to out in perp space.[63] Since we have assumed that the tiling geometry itself has even/odd symmetry, it follows that the Mn(0) portions are identical on even and odd hyperatoms, and have a shape associated with the CCT node packing, which is suspected to have a fractal boundary.[64] Of course, all orbits belonging to the MI [viz. Mn(μ), Al(α), and Al(β)] must correspond to atomic surfaces consisting of disjoint unions of the same shape, and similarly must be even/odd symmetric. The Al(α) atoms come from 6D midedge hyperatoms; such hyperatoms exist in the DO and KGme models (which contain complete MI's by construction) but are absent in the KG model.

Our δ atoms, which correspond to 6D body centers, are contained in the third shells of extended MI. In our FCI models, δ atoms are found at a radius τa_q along the fivefold axes of MI centered at *even* CCT nodes, thus realizing an atomic surface on *even* 6D body-center sites, just as in the KG and KGme models. In our FCI decoration models, certain γ-type atoms must also be removed to avoid close contacts with δ atoms; this in turn causes the γ portion of the 6D-vertex hyperatoms to exhibit an even/odd modulation.

2. 6D-cut structures as decorations?

We now turn to the reverse question: treating a 6D-cut model as a cluster packing and/or tiling decoration. Candidate MI positions can be identified as the centers of 42-atom icosidodecahedra of 6D-vertex atoms which are identical to MI second shells (such shells are common in all three of our ''standard'' 6D-cut models). Unlike the CCT, the standard 6D models contain pairs of candidate MI centers separated by ''short'' fivefold linkages of length a_q.[65] The DO and KGme models attempt to maximize the density of MI, by placing them wherever possible, but only one MI in each close pair can receive an MI. Since the CCT contains no such fivefold linkages, every CCT node can receive an MI, and so the density of MI's in our CCT-based decoration models is $\sim$10% higher than in the 6D-cut models.

In the 1/1, 2/1, and 3/2 cubic approximants to the 6D models, the short fivefold linkages are avoidable with a proper choice of centering in 6D. With this choice of centering, it turns out that the MI centers in these approximants coincide exactly with those in the corresponding CCT approximants (tilings $T1$, $T5$, and $T6$, respectively, in Table II of paper II), allowing us to overlay the 6D-cut atomic structure and the CCT tiling. This then permits an almost mechanical prescription for turning 6D models into CCT decorations: the decoration of each canonical cell simply consists of the atoms that fall into it.

Of course, this will not work for a generic quasiperiodic structure. The decoration of each cell must respect its point symmetry; furthermore, since, e.g., the 3/2 CCT approximant contains several crystallographically inequivalent C cells, it must be checked that all of them are decorated identically. The fact that it works at all for our three standard 6D-cut models (up the 3/2 cubic approximant) is the objective basis for our claim that they are similar to our CCT-based decoration models.

Following this prescription with the 3/2 approximants, the loose SI models are derived from the DO model (specifically it is decoration LS1.1, in the labeling of paper II); similarly loose FCI models are derived from the KGme model. The single difference between the 6D and the CCT versions of the approximants is the treatment of the ring of γ_Z sites on Z_{DB} faces: in the 6D models, the Al(γ_Z) atom nearest the threefold axis of the D cell is filled 50% of the time (in a deterministic way), yielding the ''5/6'' variant of the Al γ_Z ring.

Incidentally, our analysis has shown that (apart from the 6D body-center, i.e., δ-type sites) the DO and KGme models are topologically equivalent. This was not obvious to previous authors, because certain topologically equivalent atoms are assigned to different 6D Wyckoff positions in the respective models.

VI. TILE HAMILTONIANS

This section defines and develops the concept of a ''tile Hamiltonian,'' $\mathscr{H}_{\text{tile}}$, a function which assigns an energy to each allowed configuration of tiles. For the sake of simplicity/definiteness, we concentrate primarily on tile Hamiltonians for CCT-based decoration models, and we will speak only of tile-tile interactions. (It is trivial to generalize

this to interactions of generic ''tiling objects,'' as defined in Sec. II A.)

The tile Hamiltonian value $\mathscr{H}_{\rm tile}$ for a particular tiling is defined simply as the relaxed energy of the atomic structure produced by decorating that tiling. This is well defined since we have demanded that decoration always generate a unique structure.[66] It is physically meaningful (e.g., for calculating the entropy) to the extent that the tiling-structure relationship is one-to-one: that is, every low-energy structure can be generated from exactly one tiling. Notice that a change in either the decoration rule or the potentials will change $\mathscr{H}_{\rm tile}$.

There are obvious practical benefits to using $\mathscr{H}_{\rm tile}$, provided it is well defined: a large number of continuous degrees of freedom (atomic coordinates) get replaced by a much smaller number of discrete degrees of freedom (tiling configurations). Most theories about the nature of long-range order in quasicrystals are formulated as statements about the tile Hamiltonian.[19,28] In particular, a necessary and sufficient condition for the validity of the random-tiling scenario is that $\mathscr{H}_{\rm tile}$ is small compared to the effective temperature at which icosahedral order develops. Within this scenario, the phason elastic constants of the model structure can be calculated numerically by Monte Carlo simulations, using $\mathscr{H}_{\rm tile}$ as the Hamiltonian.[67]

A. Prerequisites

A generic $\mathscr{H}_{\rm tile}$ comprises one-tile terms plus intertile interactions. The tiling Hamiltonian for a given decoration model is tractable only if

(i) its intertile interactions are short range, preferably consisting only of tile-pair interactions;

(ii) the specification of these tile-pair interactions requires only a few parameters.[68]

In turn, these two criteria will be satisfied only when the decoration model is ''crystallographically good'' (as defined in Sec. II A), that is, if the relaxed positions can be well approximated by a context-independent (unrelaxed) decoration of the tiles.

Even if there are significant forces on the atoms in a given tile from atoms in the neighboring tiles, the intertile interaction can still be small, provided those forces are nearly independent of *which* tiles are neighboring. This situation is reflected in having only a small variance in the site-energy diagnostic [see paper II, Eq. (5)] over a single orbit of the decoration model. If the canonical rms σ (see Sec. II C) is small, i.e., if the atomic positions depend only weakly on which way the surrounding tiles are arranged, then the same will tend to be true for the energies.

The simplicity/usefulness of the tile Hamiltonian is related to the issue of binding (see Sec. II B). Consider first a crude decoration model, whose atoms are bound to a few basic species of tiling object. An accurate tile Hamiltonian for such a model (if one exists at all) will need to contain intertile interactions, which reflect context sensitivities (again, see Sec. II B). Now consider a more sophisticated decoration model, that is derived from the crude model by dividing each species of tiling object into several subspecies, according to the various ways in which neighboring tiling objects can be placed around it. For each such way, the atoms on the object have a distinct environment (counting second neighbors); their optimized canonical positions should, after such a rebinding, better approximate those of the relaxed structure. It should thus be possible to formulate an accurate tile Hamiltonian *without* intertile interactions. The process of rebinding thus enables the intertile interactions in the original tile Hamiltonian for the crude model to be reexpressed as (i.e., absorbed into) one-tile terms in the tile Hamiltonian for the sophisticated model.[69]

B. Subtraction of chemical potential terms

Our aim here is to formulate the simplest possible $\mathscr{H}_{\rm tile}$ for CCT-based decoration models, that correctly accounts for the energy differences between different tiling configurations. Here, we restrict our attention to CCT-based decoration models whose atoms are bound to the five species of canonical cell (see Fig. 1).

The simplest case is when $\mathscr{H}_{\rm tile}$ consists simply of one-tile terms, i.e., when it can be written in the form

$$\mathscr{H}_{\rm tile}=\sum_{\alpha} V_{\alpha}N_{\alpha}, \tag{2}$$

where N_{α} is the number of tiles of type α and V_{α} is the energy associated with each tile of that type. There are thus four independent parameters for $\alpha=A,B,D,E$ (since $N_C\equiv N_B+2N_E$). This formula can be rewritten as

$$\mathscr{H}_{\rm tile}=\mu^0_{\rm Mn}N_{\rm Mn}+\mu^0_{\rm Al}N_{\rm Al}+\sum_{\alpha} V'_{\alpha}N_{\alpha}. \tag{3}$$

Here, we have separated out two chemical-potential terms, which couple to the total number of Al and Mn atoms, $N_{\rm Al}$ and $N_{\rm Mn}$. Clearly Eq. (3) is related to Eq. (2) by $V_{\alpha}=V'_{\alpha}+\mu_{\rm Al}N^{\rm Al}_{\alpha}+\mu_{\rm Mn}N^{\rm Mn}_{\alpha}$, where $N^{\rm Al}_{\alpha}$ and $N^{\rm Mn}_{\alpha}$ are the number of Al and Mn atoms bound to tile α. There now remain only two linearly independent coefficients V'_{α}.

The values we compute here for $\mu^0_{\rm Al,Mn}$ are physically meaningless, since they omit the possibly strong effects of structure-independent terms in the total energy. The values we compute for the coefficients V'_{α}, however, constitute a measure of the deviation from a random-tiling ensemble: if both were zero, i.e., if $\mathscr{H}_{\rm tile}=\mu^0_{\rm Mn}N_{\rm Mn}+\mu^0_{\rm Al}N_{\rm Al}$, then all possible random tilings would coexist in the equilibrium state (with equal weight); in such cases, the equilibrium state could be represented as a *maximally random tiling model*.[19]

VII. SUMMARY AND DISCUSSION

Here we will review the most important parts from the preceding sections and indicate possible future developments. Since the associated computations have been left to paper II, the reader is asked to look there for results and conclusions.

A. Summary

In this paper, we have presented a general machinery for setting up (and talking about) decoration models, and a specific machinery for producing numerous variants of *i*-AlMn models, suitable for our tests using realistic pair potentials (paper II). A theme which runs through the entire work is

that *it is more desirable to understand the differences between two models than to understand the details of one model.* Another theme is the desire to dissect any model into a discrete set of orbits (i.e., types of site), since our only method for steadily improving a model is to revise one orbit at a time.

Some of the highlights of the general framework put forth in Sec. II were the notion of ''topological equivalence,'' which allowed us in passing to characterize succinctly the unrecognized near-identity of the Katz-Gratias and Duneau-Oguey structures, and the idea of a canonical rms, which provides a quantitative measure for the validity of the decoration-model positions, as approximations to the real atomic positions. The concept of binding, which we introduced Sec. II B, enables us to specify, precisely, what we mean by a decoration model. Though this concept might seem annoying in view of the onerous bookkeeping that it forces upon us (Appendix B), it is what ''dissects'' the atoms into disjoint orbits, and thus what breaks up the task of modeling the atomic structure into manageable, reasonably isolated units. Section II B also introduces the notion of ''differentiation'' of models, which clarifies how simple decoration rules may be elaborated into more complex (and more realistic) ones. This grouping of different models into a ''family tree'' gives us a precise way of describing the relationships among them.

Differentiation is used repeatedly in our actual description of the models (Sec. IV), the heart of the paper. That section shows that good decoration rules are (unexpectedly) similar to the crude and incomplete Elser-Henley rule;[24] they are also closely related to, and in part inspired by, the 6D-cut models (Sec. V). Apart from that, the geometrical details of Sec. IV are useful mainly for understanding the relaxations in paper II. Above the details, we find two suggestive concepts arising out of our structural descriptions: a new, perhaps superior set of ''dual'' rhombohedral tiles, that supply a framework for describing CCT decoration structures (Appendix A); and the view of the δ (6D body-center) sites as a lattice gas, whose fundamental parameter is its density (Sec. IV D).

Finally, we have laid out (in Sec. VI) the basic theory for constructing a ''tile Hamiltonian'' out of a decoration rule plus a function (as in our paper II) that returns the structural energy for a given atomic arrangement. This and the other above-mentioned concepts are applied in paper II, in which we both ascertain the particular models that are favored by realistic Al-Mn pair potentials, and assess the dependence of the cohesive energy on various parameters that span our space of decoration models.

B. Future directions

Here we mention some possible extensions to this work, from minor to major. (Those relating to structural energy calculations are deferred to paper II.)

1. Decorations which break inversion symmetry

One of our principles of decoration was that the decoration of a tiling object must have the same symmetry as the tiling object, but this does not necessarily describe the lowest energy state; a breaking of the local symmetry could be preferred. The main example we pursued had to do with the δ-site occupation (Sec. IV D). As discussed in Sec. II B, deviations could occur either in the form of a context sensitivity (as for δ sites in dense SI models) or in the form of a ''global symmetry breaking'' (as for δ sites in FCI models).

It might be profitable to explore breaking of the local *inversion* symmetry (which is equivalent to mirror symmetry, given the twofold axes of the icosahedral proper point group 532). For example, consider the triangle of three close γ atoms near the lower tip of PR_Y (see Sec. IV C). Instead of merging these into one γ_Y atom, or relaxing them directly outwards, it might be plausible instead to expand the triangle while rotating it a small angle clockwise or counterclockwise (so as to avoid some surrounding atoms). As in other cases, this sort of deviation might be implemented either as a context sensitivity, or as a breaking of the global inversion symmetry.

2. ''Reshuffling condition'' for kinetics?

To explain the experimental existence of well-ordered quasicrystals, it is not sufficient that they be the equilibrium phase; they must be accessible kinetically, too. If the intermediate states are valid decorated tilings, and if the decoration rules do not admit chemical disorder, this requirement poses an additional constraint on the decoration rule: atoms should be ''glissile,'' that is, they should jump only locally under tile reshufflings, to sites of the same species.[70]

We have not investigated this question for our tilings. It would be difficult to do so systematically, since the allowed rearrangement for the CCT is a nonlocal ''zipper'' move,[71] whose rules are, as yet, only partially understood. It is clear, however, that there will be a large overlap of atomic sites [an example is Ref. 58 of paper II, concerning the Mn(γ_{3D}) site].

3. Diffraction refinements

In principle, decoration models are well adapted to structural refinements and (as will be seen in a moment) demand less radical shifts from the long-established path of crystallographic refinement for a periodic crystal. Our ignorance of any infinite quasiperiodic CCT structure is only a small embarrassment for carrying out this program. One can proceed by calculating the diffraction patterns of decorated large cubic approximants; it can be confirmed that these diffraction patterns already have nearly icosahedral symmetry. Then a proper icosahedral symmetrization of the structure factors on Bragg peaks yields a very good ersatz for the diffraction pattern of an icosahedral crystal. The fitting parameters are simply the three-dimensional ''canonical'' coordinates and the chemical occupancies of each site.

As mentioned in the Introduction, such a program might profitably be combined with energy calculations. An objective function P, measuring the goodness of the adaptation of the structure to the relaxed structural energy function E_{rel} could simply be added to the R factor (which is, of course, the corresponding objective function for the fit in Fourier space between the calculated and measured structure factors). There are two plausible choices for P: the first would be simply a multiple of E_{rel}, the other would be $\Sigma\sigma_j^2$, the sum of the canonical variances.

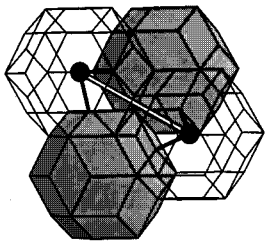

FIG. 6. The dTR triacontahedra are placed on the nodes of an *A* cell. Those on the even (odd) nodes are shown solid (in outline).

ACKNOWLEDGMENTS

This work has been supported by DOE Grant No. DE-FG02-89ER45405. We thank R. B. Phillips and and E. Cockayne for comments on the manuscript.

APPENDIX A: DUAL-RHOMBOHEDRAL (CLUSTER) APPROACH TO CCT DECORATION

The dual-rhombohedral approach decomposes the CCT into a new tiling[72] of rhombic triacontahedra and prolate rhombohedra, which we collectively call ''dual'' rhombohedra since their vertices correspond to 6D body centers [in the setting where the nodes (vertices) of the CCT come from 6D cell corners].

1. Dual-rhombohedral geometry

The decomposition of space by dual entities is very simple: on each CCT node, we center a large rhombic triacontahedron with edges of length a_q, oriented along fivefold directions. We will call this ''dTR'' (we begin the names of all dual objects with a ''d''). The dTR's always share rhombic faces along *b* linkages. Along *c* linkages, the dTR's in fact overlap by a volume congruent to an oblate rhombohedron (dOR). We show how clusters sit on the *A* cell in Fig. 6. A much larger fraction of space lies inside the dTR's of the dual decomposition than inside the RD_b plus PR_c of the vertex-rhombohedral decomposition. The union of the dTR's already accounts for 94% of the volume of the CCT (in contrast, the RD_b and PR_c in the vertex-rhombohedral description account for only 83% of the volume).

With dTR on each CCT node, the remaining gaps are all filled by dual prolate rhombohedra (dPR), of which there are two types: each *Z* face (including the internal Z_{BB} face in an *E* cell) is pierced by one dPR_Z; each *D* cell contains one dPR_D, which lies along the cell's axis of threefold symmetry. We show the placement of these dPR's in Fig. 7. In each *D* cell, the lower tip of the dPR_D and the lower tips of three dPR_Z all meet at a point on the *D* cell's threefold axis in the lower part of the cell. (We use lower, upper, front, etc., with reference to the orientations of objects as they appear in Fig. 7; this is consistent with our word usage concerning Fig. 3.)

2. Zeroth- and first-order decoration rule

Along the dual-rhombohedral path, the zeroth-order decoration is taken from the three-shell cluster shown in Fig. 2;[73] such three-shell clusters are observed in (at least) α-AlMnSi.[49,74,75] First, a Mackay icosahedron (MI) cluster is placed at the center of each dTR. Next, on the surface of each dTR, we place one γ atom on every edge, and one ''candidate'' δ site on every vertex (both threefold and fivefold vertices), except where two dTR surfaces overlap along a *c* linkage. In each such overlap, we remove the threefold candidate δ sites that lie around the *c* linkage, such that each dTR has three γ sites on its surface, which coincide with three Al(β) sites in the second (MI) shell of the other dTR.

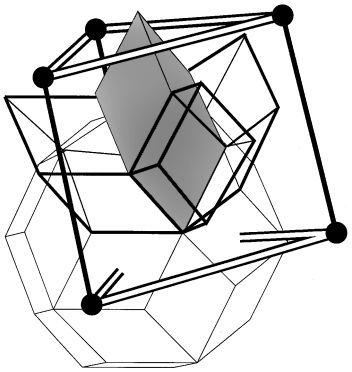

FIG. 7. Decoration of *D* cell by ''dual'' rhombohedra: (1) one dTR is shown (thin lines) surrounding the lower rear node; (2) the dPR_D appears shaded in the center; (3) surrounding it are the three dPR_Z (bold lines), centered on (and piercing through) the rectangular Z_D faces.

Since dTR's account for most of the volume, they also account for most of the atoms. Moreover, all dPR vertices are shared with dTR vertices. The rhombic faces of each dPR (both types) contain the δ and Al(γ) sites that lie on the faces of the dTR's adjoining it. Within each dPR_Z, two additional Mn(ν) sites are placed along the dPR_Z's body diagonal (threefold axis), dividing it in about the ratio $\tau^{-2}:\tau^{-3}:\tau^{-2}$.[76] The inside of each dPR_D is decorated in the same way, except that the lower Mn(ν) site is replaced by a γ_{3D} site.

The above dual-rhombohedral version of the zeroth-order description, in fact, introduces no conflicts (apart from those involved with the δ network, which were described in Sec. IV D). Hence it is also the first-order description.

It would be possible, but redundant, to describe the further options and the second-order models in dual language. It may be noted that the six γ_Z sites form a ring around the middle of dPR_Z in this representation. The δ network simply consists of all of the dual vertices, and the δ links are the edges of the rhombic faces (as in Fig. 5).

Since the δ and γ sites that experience most of the variations lie on the dTR faces, complicated decoration rules (as found in both dense families) may be conveniently visualized by taking planar projections of the surface decorations of dTR's. (In fact, it is sufficient simply to map the intersection of the dTR surface with the solid angle of each type of the CCT cell corner, as shown in Fig. 5(c) of Ref. 1.)

APPENDIX B: AN EXAMPLE OF BINDING

We present here the specification of the minimal binding for loose SI models, this being the simplest of the bindings that we implemented. We will be careful to assign each atom metrically to a tiling object so that it is accounted for once and only once, in accordance with our definition of binding.

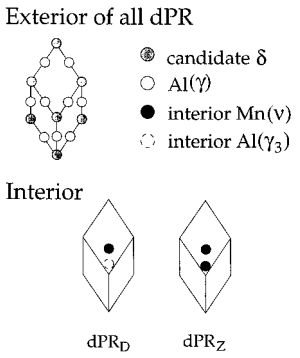

FIG. 8. Decoration of ''dual'' prolate rhombohedra by atoms. (The dTR decoration is just Fig. 2, which has faces identical to those shown here.)

We rely on the reader to visualize how this description is equivalent to the ''topological'' description presented in the text. The dense FCI and dense SI models have more elaborate bindings; at the end of this appendix, we sketch the main ways in which they differ from the loose SI binding. (Quite detailed binding descriptions for a very dense FCI model may be found in Ref. 26.)

The four orbits bound to the CCT nodes form the MI cluster. The Mn(0) site, of course, is bound to the center of the MI cluster. The 12 Mn(μ) sit on the rhombohedron vertices in an icosahedral shell of radius a_q around every CCT node. The 12 inner shell Al(α) atoms sit at the midpoints of the edges connecting Mn(0) and Mn(μ) sites. The 30 Al(β) atoms in the MI second shell divide the face diagonals of the vertex rhombohedra in the ratio $\tau^{-1}:\tau^{-2}$. The γ and δ atoms, although they often form part of the three-shell cluster illustrated in Fig. 8, can never be bound to nodes (on account of the cluster-cluster overlaps).

To each b linkage, there is assigned an orbit of 4 Al(γ_b) atoms situated near the vertical long diagonals of the rhombus faces of the RD_b in Fig. 4 (i.e., the faces in the plane of the paper). More precisely, they are situated somewhat inside the RD_b; indeed, when the RD is decomposed into two PR and two OR, the Al(γ_b) atoms are located on the long diagonals of the ''internal'' PR faces. The Al(γ) atoms shown on the ''top'' and ''bottom'' faces in Fig. 4 are not bound to the associated RD_b itself, but rather to other tiling objects. The δ_b sites are located at the intersection of the long body diagonals of the ''internal'' PR's just mentioned.

The δ_Y site is placed near the lower PR_Y tip, dividing the PR_Y diagonal in the ratio $\tau^{-2}:\tau^{-1}$; this site is bound to the Y face. The Mn(ν_Y) site is also bound to the Y face, sitting at the PR_Y's lower tip (which lies almost in the plane of the Y face). The upper part of the PR_Y is in the interior of a C or D cell; its decoration consists, respectively, of MI orbits bound to the node at the C cell's apex, and orbits bound to the D cell.

All orbits bound to the D cell involve the top half of the PR_Y, or the nearby parts of the PR_D (as seen in Figs. 3 and 4). There is an orbit of 3 Mn(ν) PR_Y sites on the PR vertices. In the first-order decoration rule, there is one pair of γ sites on each of the three upper faces of the PR_Y (on the long diagonal). However, in the loose SI family of decorations, the top three sites are always merged into one γ_{3D} orbit near the ''upper'' PR_Y tip, dividing the PR_Y body diagonal in the ratio $\tau^{-3}:1-\tau^{-3}$. Another orbit consists of the Al(γ_{D1}) atoms on the three faces, dividing the face diagonals in the ratio $\tau^{-1}:\tau^{-2}$. There is also one (candidate) δ_D site on the body diagonal of each of the three PR_D in the D cell.

The γ_Z sites will account for all remaining atoms in the B, D, and E cells. The six Al(γ_Z) sites decorating each OR_Z in the vertex-rhombohedral tiling are always sited at 6D body-center midedge (BCME) locations, sitting on the bisecting plane of the OR_Z associated with every Z face. They sit on the line running from the midpoint of the threefold axis to that of each edge, dividing it in the ratio $\tau^{-1}:\tau^{-2}$.

In fact, the Al(γ_Z) are rebound in several different orbits, first to respect the symmetries of the respective tiling objects in which the OR_Z finds itself, and second to facilitate variations of the decoration rule in which certain γ_Z sites are left vacant (an example of context sensitivity, as defined in Sec. II B).

The six Al(γ_Z) sites inside the highly symmetric E cell are bound to it, forming just one orbit. The other Al(γ_Z) sites could be bound to Z_D faces, which occur between two D cells, and between a D and a B cell. (A binding to the Z_D object, which lacks sixfold symmetry, would require two separate orbits.) However, due to certain technicalities in our algorithm for identifying tiling objects (given the node locations), it was more convenient to further differentiate the Z_D face into classes Z_{DD} (treated like the Z_D) and Z_{DB}. The orbits of the Z_{DB} may be bound to the B cell, in which case three separate orbits are needed to account for the six Al (γ_Z) sites.

This completes the binding description of the Loose SI decoration; it is summarized in Table IV, which can be used to compute the number of atoms of each class in a given CCT tiling. Chemical variations may be performed for the orbits δ_Y and γ_{3D} independently. The density variations are realized by filling/emptying the δ_Y sites and by choosing either the ''4/6'' or the ''6/6'' option for the ring of six Al (γ_Z) sites associated with each Z_D face (see paper II). These variant models are easily constructed from the basic binding formulation given above, since each variation affects only one orbit.

The dense FCI model is more complicated because it differentiates many types of tiling object into odd and even flavors. As a result, the number of distinct orbits almost doubles. Indeed, the minimal binding requires 20 orbits of atoms bound to seven types of (even- or odd-) flavored CCT objects; a typical binding that differentiates some of the problematic orbits (by rebinding them to objects of lower symmetry) has a total of 38 orbits for nine CCT objects. [In this rebinding, the Al(δ) of the odd b linkages are rebound to the A, B, D, and E cells into which they fall; and the γ_{3Y} of the odd Y face are rebound to the B, D, and E cells into which they fall.]

The dense SI decorations are complicated in a different way. In these (see Sec. IV E 2) we adopted an alternative strategy for occupying δ_b sites, such which they were subdivided into three subclasses according to the neighboring tiles sharing the b linkage. Correspondingly, then, the b linkages adjacent to the faces of A cells marked ''-'' in Fig. 1(b) of Ref. 1 are differentiated into three new tiling objects

$b(A_4)$, $b(A_2)$, and $b(A_{CC})$. Then the γ_b and δ_b sites for these b linkages are rebound to these three new tiling objects (called $b(A_4)$, $b(A_2)$, and $b(A_{CC})$, since they depend upon the surrounding A cells). The other b linkages are no longer used for decoration: all of their γ_b atoms (and δ_b atoms, if any) are rebound to Y faces and other CCT objects. A minimal binding specification for the dense SI model requires (typically) 22 orbits bound to nine CCT tiling objects.

*Permanent address: Institute of Physics, Slovak Academy of Sciences, Dubravska cesta 8, 842 28 Bratislava, Slovakia.

†Present address: Department of Physics, Theoretical Physics, 1 Keble Road, Oxford, OX1 3NP, England.

[1] C. L. Henley, Phys. Rev. B **43**, 993 (1991).

[2] M. Mihalkovič, W.-J. Zhu, C. L. Henley, and R. Phillips, following paper, Phys. Rev. B **53**, 9021 (1996). Brief preliminary reports of our work have appeared in M. Mihalkovič, W.-J. Zhu, C. L. Henley, M. E. J. Newman, M. Oxborrow, and R. B. Phillips, in *Aperiodic '94*, edited by G. Chapuis and W. Paciorek (World Scientific, Singapore, 1995), p. 169 and W.-J. Zhu, C. L. Henley, and M. Mihalkovič, in *Proceedings of ICQ5*, edited by J.-M. Dubois (World Scientific, Singapore, in press).

[3] J. W. Cahn, D. Gratias, and B. Mozer, J. Phys. (Paris) **49**, 1225 (1988).

[4] M. Duneau and C. Oguey, J. Phys. (Paris) **50**, 135 (1989).

[5] C. Janot, J.-M. Dubois, M. de Boissieu, and J. Pannetier, Physica B **156&157**, 25 (1989).

[6] A. Yamamoto, in *Quasicrystals*, edited by T. Fujiwara and T. Ogawa, Springer Series in Solid State Sciences Vol. 93 (Springer-Verlag, Berlin, 1990), p. 57.

[7] M. de Boissieu, C. Janot, J.-M. Dubois, M. Audier, and B. Dubost, J. Phys. Condens. Matter **3**, 1 (1991).

[8] A. Yamamoto, Phys. Rev. B **45**, 5217 (1992).

[9] M. Cornier-Quiquandon, A. Quivy, S. LeFebvre, E. Elkaim, G. Heger, A. Katz, and D. Gratias, Phys. Rev. B **44**, 2071 (1991).

[10] A. Katz and D. Gratias, J. Non-Cryst. Solids **153&154**, 187 (1993).

[11] A. Katz and D. Gratias, in *Lectures on Quasicrystals*, edited by F. Hippert and D. Gratias (Les Editions de Physique, Les Ulis, France, 1994), p. 187.

[12] E. Cockayne, R. Phillips, X.-B. Kan, S. C. Moss, J. L. Robertson, T. Ishimasa, and M. Mori, J. Non-Cryst. Solids **153&154**, 140 (1993).

[13] M. Boudard, M. de Boissieu, C. Janot, J. M. Dubois, and C. Dong, Philos. Mag. Lett. **64**, 197 (1991); M. de Boissieu, P. Stephens, M. Boudard, C. Janot, D. L. Chapman, and M. Audier, J. Phys. Condens. Matter **6**, 10 725 (1994).

[14] C. Janot, M. de Boissieu, J. M. Dubois, and J. Pannetier, J. Phys. Condens. Matter **1**, 1029 (1989).

[15] The realistic pair potentials, however, have quite important second-neighbor interactions. (See paper II.)

[16] M. de Boissiieu, P. Guyot, and M. Audier, in *Lectures on Quasicrystals* (Ref. 11), p. 1.

[17] M. de Boissieu, C. Janot, and J.-M. Dubois, J. Phys. Condens. Matter **2**, 2499 (1990).

[18] C. L. Henley, in *Quasicrystals and Incommensurate Structures in Condensed Matter*, edited by M. J. Yacaman, D. Romeu, V. Castaño, and A. Gómez (World Scientific, Singapore, 1990) p. 152; M. Widom, in *Quasicrystals*, edited by M. V. Jarić and S. Lundqvist (World Scientific, Singapore, 1990), p. 337.

[19] C. L. Henley, in *Quasicrystals: The State of the Art*, edited by D. P. DiVincenzo and P. J. Steinhardt (World Scientific, Singapore, 1991), p. 429.

[20] M. de Boissieu, P. Stephens, M. Boudard, C. Janot, D. L. Chapman, and M. Audier, Phys. Rev. Lett. **72**, 3538 (1994); M. de Boissieu, M. Boudard, B. Hennion, R. Bellissent, S. Kycia, A. Goldman, C. Janot, and M. Audier, Phys. Rev. Lett. **75**, 89 (1995).

[21] The case of i-AlPdMn furnishes a good example of the need for structural refinement based on both cohesive-energy calculations and diffraction data: The diffraction data (Ref. 13) do not resolve the positions of the inner Al shell of the (pseudo)-MI cluster (see Sec. III B); in contrast, cohesive energy calculations could give reliable information about these sites (since the surrounding second-shell sites are known). On the other hand, cohesive-energy calculations run into difficulties if asked to determine the occupancy of "δ" (6D body-center) sites, since the contribution to the cohesive-energy from these sites is extremely sensitive to the precise shapes of the tails of the relevant pair potentials (see Ref. 2); in contrast, diffraction data (Ref. 13) clearly show that Pd atoms occupy the δ sites.

[22] E. Cockayne, M. Widom, P. Launois, M. Fettweis, and F. Dénoyer, in *Aperiodic '94* (Ref. 2), p. 578.

[23] M. Mihalkovič, M. Oxborrow, and C. L. Henley (unpublished).

[24] V. Elser and C. L. Henley, Phys. Rev. Lett. **55**, 2883 (1985).

[25] M. Mihalkovič and P. Mrafko, Phys. Rev. B **49**, 100 (1994).

[26] M. Oxborrow, Ph. D. thesis, Cornell University, Ithaca, 1993.

[27] L.-H. Tang and M. V. Jarić, Phys. Rev. B **41**, 4524 (1990).

[28] H.-C. Jeong and P. J. Steinhardt, Phys. Rev. Lett. **73**, 1943 (1994).

[29] A more precise term for this relationship might be "relaxation equivalent." It is not the same as (e.g.) the equivalence (as graphs) of the nearest-neighbor bond networks produced by the Voronoi construction.

[30] V. Elser, Phys. Rev. B **32**, 4892 (1985).

[31] In a 6D description, this is accomplished by allowing a "parallel-space displacement" $\mathbf{x}^{\parallel}(\mathbf{x}^{\perp})$, where $\mathbf{x}^{\parallel}$ is a function of the position within the hyperatom, denoted by $\mathbf{x}^{\perp}$. See Ref. 17.

[32] The Mn(0) site, located at and bound to the CCT node, is the only site whose canonical displacement is zero by symmetry, hence its space of canonical displacements is 0 dimensional. A more typical example is the δ_Y site, which, in our minimal decoration model (Sec. IV and Appendix B), is bound to the Y face's axis of threefold symmetry. Its space of canonical displacements is restricted to translations along this axis, and thus is one-dimensional.

[33] An additional technical benefit of using ideal sites is that the model has a small set of possible interatomic vectors, and hence a not too large set of possible coordination shells. It also biases us towards models in which rearrangements of tiles correspond to relatively few rearrangements of atoms, since the ideal coordinates of many atoms will be unchanged by the tile flips.

[34] M. Mihalkovič and P. Mrafko, Philos. Mag. Lett. **69**, 85 (1994).

[35] A canonical-cell model for i-TiMn, with complete Bergman clusters, has been formulated by M. Mihalkovič (unpublished); see also Ref. 45.

[36] M. E. J. Newman, C. L. Henley, and M. Oxborrow, Philos. Mag. B **71**, 991 (1995).

[37] Certain growth models are practically CCT's: see J. L. Robertson and S. C. Moss, Phys. Rev. Lett. **66**, 353 (1991); Z. Phys. B **83**, 391 (1991).

[38] An ''n-fold direction'' (where n equals either 2, 3, or 5) points along an axis of n-fold rotational symmetry with respect to an icosahedron, whose center the axis passes through.

[39] The distance between nearest-neighbor nodes along threefold linkages is $(3\tau^3/\sqrt{5})^{1/2}a_q \approx 11.0$ Å, and the distance between nearest-neighbor nodes along twofold linkages is $2(\tau^3/\sqrt{5})^{1/2}a_q \approx 12.7$ Å.

[40] If we represented this particular arrangement of nodes as a combination of two B cells, there would be three possible placements of the Z face, for the same placement of nodes. Thus, we demand that this arrangement always be called an E cell. (It follows that, on the tiles we continue to admit as B tiles the Z faces are *always* shared with D tiles.) The E cell was called a ''B_2'' cell in Ref. 1.

[41] Although that is what the abbreviation stands for, our MI cluster is somewhat different from the true ''Mackay icosahedron'' (a finite icosatwinning of the fcc lattice). Our MI always contains only the first two shells of Mackay's cluster, whose atomic sites are filled by Al and Mn as in Fig. 2.

[42] Y. Ma and E. A. Stern, Phys. Rev. B **38**, 3754 (1988); A. Sadoc, A. M. Flank, and P. Lagarde, Philos. Mag. B **57**, 399 (1988).

[43] M. Boudard, M. de Boissieu, and C. Janot, Europhys. Lett. **22**, 181 (1993).

[44] G. Bergman, J. L. T. Waugh, and L. Pauling, Acta Crystallogr. **10**, 254 (1957).

[45] C. L. Henley and V. Elser, Philos. Mag. Lett. B **53**, L59 (1986).

[46] C. L. Henley, in *Quasicrystals*, edited by T. Fujiwara and T. Ogawa, Springer Series in Solid State Sciences Vol. 93, (Springer, Berlin, 1990), p. 38.

[47] If one compiles lists of nearest Mn-Mn neighbor distances in each structure, it turns out that the variance of this distance typically reaches its minimum near the quasicrystal-forming value of $x_{\mathrm{Mn}} \approx 0.20$. [C. L. Henley, (unpublished).]

[48] J. Zou and A. E. Carlsson, Phys. Rev. Lett. **70**, 3748 (1993).

[49] H. A. Fowler, B. Mozer, and J. W. Cahn, Phys. Rev. B **37**, 3906 (1988).

[50] D. P. Shoemaker and C. B. Shoemaker, in *Introduction to Quasicrystals*, edited by M. V. Jarić (Academic, San Diego, 1988), p. 1.

[51] C. L. Henley, Philos. Mag. Lett. **58**, 87 (1988).

[52] N. K. Mukhopadyay, S. Ranganathan, and K. Chattopadhyay, Philos. Mag. Lett. **60**, 207 (1989).

[53] The distinction between successive ''levels of description'' is not mathematically precise; it is more a statement of the way in which we organize our description of the model.

[54] An initial attempt to extend the Elser-Henley rule makes full usage of the empirical structural knowledge from α-AlMnSi and α-AlFeSi, namely that Mn atoms are spaced as uniformly as possible (with mean spacing ~ 4.6 Å). First MI clusters are placed at CCT nodes; Mn(ν) sites are then defined at the intersections of (several) spheres of radius $a_q = 4.6$ Å, drawn around Mn(μ) atoms, and finally Al atoms are filled in. This produces a decoration similar to the vertex-rhombohedral approach; the most important variation was the possibility of making the tetrahedron of four Mn(ν) on the upper end of the $\mathrm{PR}_Y(D)$ part of an $\mathrm{Al_6Mn_4}$ tetrahedron motif.

[55] Ref. 45 is just such a model for the Frank-Kasper family of quasicrystals.

[56] C. L. Henley, Phys. Rev. B **34**, 797 (1986).

[57] A few γ sites become vacant, or merge together to a new site which is somewhat displaced sideways from the midpoint (as in the γ_{3D} and γ_Z cases).

[58] The δ sites at the fivefold vertices of those dTR that are centered on even (odd) CCT nodes are defined to be even (odd). Given this convention, it turns out that the δ_b sites associated with ''even'' b linkages are odd, and thus remain unoccupied in (dense) FCI decorations.

[59] The variants involving γ sites may also be preselected according to the biases (in opposite directions) which enter the building of ''dense'' or ''loose'' rules. For example, among the variants of dense models which were actually relaxed in paper II, the OR_Z rhombohedra always took the ''6/6'' option.

[60] R.N. Corby and P.J. Black, Acta Crystallogr. B **33**, 3468 (1977).

[61] All Fe sites are set to Mn; all Cu sites, which originate from the KG model's body-center motif (atomic surface), are set to either all Al or all Mn, depending on the particular variant in question; all Al sites remain Al.

[62] We identify environments by counting the number of neighbors at each of the seven different distances listed in Table III. This method would fail to distinguish environments with inequivalent coordination shells that happen to have the same number of neighbors at each of these seven distances.

[63] Though it is often convenient to attribute certain γ atoms to 6D body-center midedge (BCME) sites, there are usually alternate, topologically equivalent ideal positions for these atoms on 6D vertex sites; the latter way is more convenient for comparison to 6D models.

[64] E. Cockayne, Phys. Rev. B **49**, 993 (1994).

[65] The network of these potential MI centers is very similar to the 12-fold vertex network within the Ammann tiling (3DPT) studied in Ref. 56.

[66] Here, we ignore the possibility of spontaneous symmetry-breaking under relaxation — see Sec. VII B 1.

[67] At $T > 0$, the ''tile Hamiltonian'' ought to incorporate the free energy of vibrations of atoms: if some modes are rather local, their frequencies may be different depending on the tiling environment.

[68] For example, if an independent energy were associated with each of the 32 ways of packing canonical cells around a node, the model would be extremely complicated; moreover, the determination of its free parameters would require calculating the cohesive energy for more than the 11 tilings that we considered in paper II.

[69] It should be noted, however, that this dramatic simplification is somewhat cosmetic: from a computational standpoint, the evaluation of intertile interactions and the recognition of complicated tiling objects are similar (if not totally equivalent) tasks.

[70] We thank V. Elser (personal communication) for persuading us as to the importance of this point (see Ref. 19, Sec. 11.8). It has been put independently by Katz and Gratias in Ref. 11; their notion of ''glissile'' atoms is specific to quasiperiodic models, but its extension to random tilings is clear. In 6D models the only allowed phason rearrangements are implemented by translating the cut plane continuously in the ''perp'' direction; thus the ''glissile'' constraint implies the ''glueing'' or ''closeness'' condition, which requires that the boundaries of the atomic surfaces be connected (almost everywhere) by additional hypersurfaces lying purely in the perp subspace. [See P. A. Kalugin, Europhys. Lett. **9**, 545 (1989).]

[71] M. Oxborrow and C. L. Henley (unpublished).

[72] Strictly speaking, the dual rhombohedra form not a ''tiling'' but a

''covering'' since the dTR's overlap along threefold linkages.

[73] Note that our labeling of site types in the zeroth-order model (by Greek letters) appears even simpler in the dual-rhombohedral description, since each letter corresponds to one kind of position on the three-shell cluster.

[74] The third shell in α-AlMnSi or i-AlMn was previously represented as a triacontahedron on p. 11 of M. Audier and P. Guyot, in *Extended Icosahedral Structures*, edited by M. V. Jarić (Academic, San Diego, 1989).

[75] The same approach would be equally good for the i-AlCuLi structure, in which a three-shell cluster is already well known. See M. Audier, P. Sainfort, and B. Dubost, Philos. Mag. B **54**, L105 (1986); and M. Audier and P. Guyot, in *Quasicrystalline Materials*, edited by Ch. Janot and J. M. Dubois (World Scientific, Singapore, 1988), p. 181.

[76] Intriguingly, this is identical to the decoration of *vertex* prolate rhombohedra in the Henley-Elser model for Frank-Kasper quasicrystals, Ref. 45; this unexpected relationship to such models plays a prominent role in the model for i-TiCrSi of Ref. 35. See also V. E. Dmitrienko, in *Proceedings of ICQ5* (Ref. 2).